

Evaluation of a new lightning-produced NO_x parameterization for cloud resolving models and its associated uncertainties

C. Barthe^{1,*} and M. C. Barth¹

¹National Center for Atmospheric Research, Boulder, CO, USA

* now at: Laboratoire d'Aérodynamique, CNRS/Université Paul Sabatier, Toulouse, France

Received: 18 February 2008 – Published in Atmos. Chem. Phys. Discuss.: 4 April 2008

Revised: 3 July 2008 – Accepted: 15 July 2008 – Published: 18 August 2008

Abstract. A new parameterization of the lightning-produced NO_x has been developed for cloud-resolving models. This parameterization is based on the unique characteristics of identifying which convective cells are capable of producing lightning based on a vertical velocity threshold and estimating the lightning flash rate in each convective cell from the non-precipitation and precipitation ice mass flux product. Further, the source location is filamentary instead of volumetric as in most previous parameterizations.

This parameterization has been tested on the 10 July 1996 Stratospheric-Tropospheric Experiment: Radiation, Aerosols and Ozone (STERA0) storm. Comparisons of the simulated flash rate and NO mixing ratio (control experiment) with observations at different locations and stages of the storm show good agreement. An individual flash produces on average 121 ± 41 moles of NO ($7.3 \pm 2.5 \times 10^{25}$ molecules NO) for the simulated high cloud base, high shear storm that is dominated by intra-cloud flash activity. Sensitivity tests have been performed to study the impact of the flash rate, the cloud-to-ground flash ratio, the flash length, the spatial distribution of the NO molecules, and the production rate per flash on the NO concentration and distribution. Results show a strong impact from the flash rate, the spatial placement of the lightning- NO_x source and the number of moles produced per flash. On the other hand, the simulations show almost no impact from the different cloud-to-ground (CG) ratios and the lightning- NO_x production rates per CG flash used as input to the model.

1 Introduction

Lightning flashes are considered to be a major source for nitrogen oxides ($\text{NO}_x = \text{NO} + \text{NO}_2$) in the upper troposphere. However, large uncertainties remain for their production rate both at the local and global scales. A recent review of the global lightning-produced NO_x (LNO_x) source (Schumann and Huntrieser, 2007) states that a typical storm produces $2\text{--}40 \times 10^{25}$ NO molecules per flash. In their review, Schumann and Huntrieser (2007) suggest that the global production estimate from observations and chemistry-transport models (CTM) is likely $2\text{--}8 \text{ Tg(N) yr}^{-1}$.

Results of cloud-resolving models (CRM) can be used to derive the production rate of NO per flash, the relative contribution of intra-cloud and cloud-to-ground flashes (DeCaria et al., 2005; Ott et al., 2007), the vertical profile of LNO_x (Pickering et al., 1998; DeCaria et al., 2005), and the geographical flash rate for use in CTMs. Two approaches for diagnosing LNO_x production in CRMs can be distinguished. First, the LNO_x production can be deduced from an explicit electrical scheme (Zhang et al., 2003; Barthe et al., 2007b) in which the lightning flash path is explicitly computed. This approach allows distributing the NO at the exact location of the simulated flash path, but complete explicit electrical schemes (cloud electrification and electric charge neutralization by lightning discharges) are only available in a few models (Helsdon et al., 1992; Mansell et al., 2002; Barthe et al., 2005). Second, a parameterization of the LNO_x production can be used. In the last decade, several LNO_x parameterizations have been developed for CRMs. One of the first parameterizations was developed by Pickering et al. (1998) using the Goddard Cumulus Ensemble cloud model with further improvements by DeCaria et al. (2000, 2005) and Ott et al. (2007). Other parameterizations have been implemented in MM5 (Fehr et al., 2004) or in the Wang and Chang (1993) model (Wang and Prinn, 2000). For each component of the



Correspondence to: C. Barthe
(christelle.barthe@aero.obs-mip.fr)

LNO_x production (flash rate, spatial distribution of the NO molecules, amount of NO produced per flash), different parameterizations are available.

A flash discharge can either reach the ground (cloud-to-ground discharge or *CG*) or not (intra-cloud discharge or *IC*). As these two types of discharges have different behavior, they should be considered separately. The total flash rate can be determined from an empirically derived formula based on the maximum vertical velocity (Price and Rind, 1992), which has been used by Pickering et al. (1998) and Fehr et al. (2004). In the disk model of Wang and Prinn (2000), the flash rate is derived from the collision rate between ice crystals and graupel. Another option is to use the observed total flash rate when it is available as done by DeCaria et al. (2000, 2005) and Ott et al. (2007). The advantage of using observations is that they can be used to identify whether the flash is cloud-to-ground or intra-cloud (DeCaria et al., 2000, 2005; Ott et al., 2007). However, observations of total lightning for a particular storm are difficult to obtain because ground-based networks (NLDN in the U.S., Meteorage and BLIDS in Europe) typically record *CG* flashes primarily. In other studies, the *CG* flash rate is derived either from the depth of the layer from the freezing level to the cloud top height (Price and Rind, 1992; Pickering et al., 1998; Fehr et al., 2004) or deduced from global observations (Wang and Prinn, 2000).

The spatial distribution of the NO molecules in the cloud is of primary importance as it will influence how and where the NO is transported and reacts chemically. The vertical distribution of the NO molecules in the models is either uniform (Pickering et al., 1998; Fehr et al., 2004) or follows a bimodal and Gaussian distribution for *IC* and *CG* flashes, respectively (DeCaria et al., 2000, 2005; Ott et al., 2007). If the vertical distribution is uniform, the NO produced by cloud-to-ground discharges is distributed below the -15°C isotherm and above the -15°C isotherm when produced by intra-cloud flashes. The way the LNO_x is horizontally distributed also differs from one parameterization to another. The simplest way consists of distributing the NO molecules horizontally in the whole cloud or within the 20 dBZ contour (Pickering et al., 1998; DeCaria et al., 2000, 2005). Fehr et al. (2004) chose randomly one column in the cloud with mixing ratio higher than a threshold where NO would be deposited. The most sophisticated horizontal distribution is the one of Ott et al. (2007) who attempted to mimic the tortuous aspect of the lightning channel. In their model, the number of points where the NO is deposited vertically follows the bimodal distribution, and the points where the NO molecules are distributed is chosen randomly among possible points located in a predetermined area downwind of the convective core. With this approach, the NO is no longer instantly diluted in a large volume of the cloud, but it is distributed in a region where lightning flashes are expected to propagate.

The lightning flash length contributes to the amount of NO produced from lightning. Previous studies have used an av-

eraged flash length either for the storm or for segments of the storm. For example, Ott et al. (2007) used the average hourly length per flash calculated for the 21 July European Lightning Nitrogen Oxides Project (EULINOX) storm as given by Théry et al. (2000) (21.5, 27.9 and 31.4 km). For the 10 July 1996 STERAO storm, Defer et al. (2003) reported an average flash length of 19 km but with the flash length values ranging from 0.02 to 474 km.

The last step of a LNO_x parameterization is prescribing the magnitude of NO produced by lightning flashes. Pickering et al. (1998) adopted the Price et al. (1997) values (6.7×10^{26} molecules NO per *CG*=1113 moles NO per *CG* and 6.7×10^{25} molecules per *IC*=111 moles NO per *IC*) assuming that a cloud-to-ground flash produces ten times more NO molecules than an intra-cloud flash. Wang and Prinn (2000) tested both the Price et al. (1997) values and the Franzblau and Popp (1989) values (3.0×10^{27} molecules of NO per *CG*=4982 moles NO per *CG* and 3.0×10^{26} molecules of NO per *IC*=498 moles NO per *IC*). The Franzblau and Popp (1989) values produced very high modeled NO mixing ratios in the Wang and Prinn (2000) study and has since been noted to be an abnormally high NO production rate (Salzmann et al., 2008). DeCaria et al. (2005) used the method of Price et al. (1997) to deduce the production rate per *CG* in the 12 July 1996 STERAO storm. To deduce the production rate per *IC*, they performed several simulations with different ratios between the production rate per *IC* and the production rate per *CG*. They concluded that taking a production rate of NO per *IC* that is 75 to 100% of the production rate of NO per *CG* best matches with observations. Using the same method, Ott et al. (2007) deduced that a production rate of 360 moles of NO per *IC* and *CG* compares favorably with observations for the 21 July 1998 EULINOX storm. For this same storm, Fehr et al. (2004) concluded that the flash production rates suggested by Price et al. (1997) are not supported by the analysis. They estimated the *CG* and *IC* production rates to be 2.1×10^{26} molecules NO (349 moles NO) and 2.9×10^{26} molecules NO (482 moles NO), respectively. The recent results of DeCaria et al. (2000, 2005), Fehr et al. (2004) and Ott et al. (2007) are in agreement with Ridley et al. (2005) who suggested that *CG* and *IC* flash may produce approximately the same amount of NO per flash. Drawing a general conclusion from these previous studies is further complicated because of the use of different models in which other model parameters can affect the results and by simulations of different storms. Sensitivities of the results to individual parts of the LNO_x parameterization is best accomplished within the same model framework, while variations among models can be assessed via intercomparison studies.

Barth et al. (2007b) reported the results of an intercomparison exercise partly dedicated to the production of NO by lightning flashes. The storm of 10 July 1996 during the STERAO campaign was simulated by eight different models. Two of the models used an explicit electrical scheme

(Helsdon et al., 1992; Barthe et al., 2005) coupled to a NO production by lightning flashes (Zhang et al., 2003; Barthe et al., 2007b). Four other models used the parameterizations of Pickering et al. (1998), DeCaria et al. (2005) and Wang and Prinn (2000), while the remaining two models did not include a lightning production of NO parameterization. For the same storm, estimated values of the NO production by lightning flashes range from 36 moles fl⁻¹ to 465 moles fl⁻¹ for intra-cloud discharges, and 36 moles fl⁻¹ to 1113 moles fl⁻¹ for cloud-to-ground discharges. The models that predicted the lower LNO_x production rates are the ones using explicit electrical schemes, which placed the lightning-produced NO source in a small volume along the simulated lightning flash (filamentary) and reproduced the observed peaks and flux quite well for this storm. Since the other models distribute the NO in a large volume, these results tend to suggest that the position of the flash and its spatial distribution (vertical and horizontal) is fundamental in modeling LNO_x at the cloud scale.

Despite some studies that investigated the impact of the relative contribution of intra-cloud and cloud-to-ground discharges to the LNO_x production (DeCaria et al., 2000, 2005; Ott et al., 2007), few have been made to understand the relative impact of different choices for the different steps of the LNO_x parameterizations. The objectives of this paper are to introduce a new LNO_x parameterization and to evaluate the sensitivity of the LNO_x parameterization to lightning parameters (flash rate, flash length, spatial distribution of the NO molecules, presence of short duration flashes) through a series of sensitivity studies. A new parameterization for the LNO_x production is presented in Sect. 2. The model framework and configuration and the studied storm are described in Sect. 3. In Sect. 4, the reference simulation is studied, and the sensitivity tests are presented in Sect. 5.

2 Description of the lightning-produced NO_x parameterization

The goal of this new parameterization is to predict the temporal and spatial distribution of individual lightning flashes without using a computationally explicit electrical scheme. Except for the explicit electrical schemes (Zhang et al., 2003; Barthe et al., 2007b), LNO_x parameterizations distribute the NO molecules either where the radar reflectivity exceeds 20 dBZ or within cloudy regions where the temperature is colder than -15°C (Pickering et al., 1998; DeCaria et al., 2000). A first approach has been made by Ott et al. (2007) to simulate the filamentary aspect of a lightning flash. The parameterization presented here builds on this approach by estimating the lightning activity in each individual convective cell rather than the entire storm. This LNO_x parameterization is then intermediate between the explicit treatment of the lightning and the more global approach of previous parameterizations.

When several convective cells are present, they may not all produce lightning flashes despite having radar reflectivity greater than 20 dBZ or cloud top colder than -15°C. An algorithm has been developed to detect potentially electrified cells. In order for lightning flashes to occur, the updraft speed must exceed 15 m s⁻¹ which is based on the 10–12 m s⁻¹ threshold estimated by Zipser and Lutz (1994) for tropical convection observed over both ocean and land in Australia and compared to electrified midlatitude continental convection observed over the central U.S.

Unique to this parameterization is the prediction of lightning flash rate based on the fluxes of non-precipitating and precipitating ice. Through theoretical and observational investigations, Blyth et al. (2001), Deierling (2006) and Latham et al. (2007) have shown a strong correlation between the total flash rate and the precipitation and non-precipitation ice mass flux product which is called the flux hypothesis. Barthe et al. (2007a) (hereinafter referred to as BDB07) show that simulated ice mass flux product for the entire storm is quite similar to the ice mass flux product derived from radar observations. In this study, the parameterization is improved by calculating the non-precipitation and precipitation ice mass flux product for each individual convective cell and is associated to a total flash rate per cell. Thus, the initial equation of BDB07 has been slightly modified to take into account the computation of the total flash rate per individual cell.

$$F_{MF} = 1.13 \times 10^{-15} \times f_{np} \times f_p \quad (1)$$

where F_{MF} is the total flash rate (fl. min⁻¹) computed from the precipitation and non-precipitation ice mass fluxes, f_p (kg m s⁻¹) and f_{np} (kg s⁻¹), respectively. The 1.13×10^{-15} coefficient has been determined from comparisons between model results and lightning and radar data. BDB07 used this coefficient for calculating the flash rate of two STERAO storms. For both storms the calculated flash rate agreed well with the observed lightning flash rates.

The flash triggering and propagation is based on Ott et al. (2007). Flashes can be triggered in the region downwind of the maximum vertical velocity (Proctor, 1981; Christian et al., 1999; Ushio et al., 2003; Ott et al., 2007). This region is defined by the convective core and by the region extending 10 km downwind of the maximum vertical velocity (C_{trig}) (Fig. 1). The downwind direction is assumed to be the mean wind direction at the altitude where both non-precipitation and precipitation ice particles are encountered. The center of the region where an individual flash can propagate is chosen randomly among all the points of the cylinder that are in the glaciated part of the cloud. Another cylinder C_{prop} where a lightning flash can propagate (radius 4 km but could depend on the flash length) is centered on the randomly chosen point. The radius of the cylinder is based on Ott et al. (2007) who found a 5 km horizontal extent from analysis of the EULI-NOX interferometer data. The points of the cylinder where the discharge can propagate are restricted to the region of the

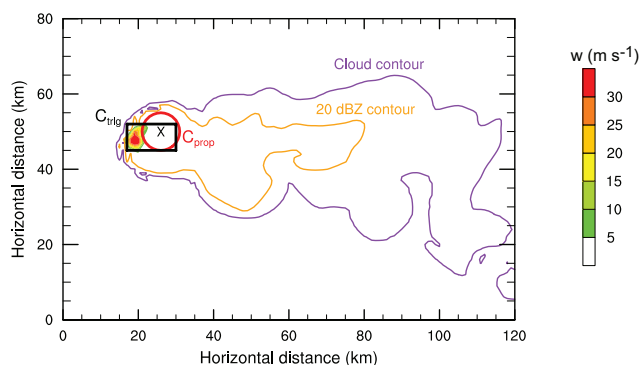


Fig. 1. Horizontal cross section at 9.5 km m.s.l. during the supercell stage ($t=2\text{h}30$) of the vertical velocity (m s^{-1} ; colored area). The black rectangle, the black cross and the red circle represent the region where a flash can be initiated (C_{trig}), the triggering point of an individual flash and the horizontal area over which the flash can extend (C_{prop}), respectively. The cloud contour (purple line) and the 20 dBZ contour (orange line) are also represented. The cloud contour is defined as the total hydrometeor mixing ratio higher than $1 \times 10^{-5} \text{ kg kg}^{-1}$.

cloud where ice particles can be found since the hydrometeors that carry most of the electric charges are the ice particles (Barthe and Pinty, 2007a).

The vertical distribution of the flash channel follows a bimodal distribution (DeCaria et al., 2000, 2005; Ott et al., 2007) peaking at -50°C and -15°C . This kind of structure is the most commonly observed (Shao and Krehbiel, 1996; Krehbiel et al., 2000; Rison et al., 1999; Thomas et al., 2001; Wiens et al., 2005; Bruning et al., 2007) and simulated by explicit electrical schemes (Mansell et al., 2002; Barthe and Pinty, 2007b). For each altitude level, the grid points reached by the lightning channel are chosen randomly among the possible points in the cylinder C_{prop} to mimic the filamentary and tortuous aspect of a lightning flash (Ott et al., 2007). The flash length of the lightning flash is prescribed either to be constant or to have a lognormal distribution (Defer et al., 2003; Pinty and Barthe, 2008).

The amount of NO produced per flash is assumed to depend on the flash length and on the altitude based on a laboratory study (Wang et al., 1998):

$$n_{\text{NO}}(P) = a + bP \quad (2)$$

with n_{NO} the number of NO molecules produced per flash length (molecules m^{-1}), P the pressure (Pa). Wang et al. (1998) set the coefficients to $a=0.34 \times 10^{21}$ and $b=1.30 \times 10^{16}$. However, a wide range ($1\text{--}13 \times 10^{21}$ molecules NO m^{-1} of flash) has been determined from observations, laboratory experiments or modeling studies (Höller et al., 1999; Stith et al., 1999; Huntrieser et al., 2002; Skamarock et al., 2003; Ott et al., 2007).

The aim of this new parameterization is to reproduce the global morphology of a lightning flash in terms of spatial

distribution and length in order to avoid the instantaneous dilution of the NO in the storm. This is important for the redistribution of the chemical species and for the comparison between model results and observations.

3 Experimental and model design

The lightning-produced NO_x parameterization described above has been placed in the Weather Research and Forecasting (WRF) model. Simulations of the 10 July 1996 STERAO storm have been conducted to evaluate and assess its sensitivities.

3.1 The WRF model

The WRF model solves the conservative (flux-form), non-hydrostatic compressible equations using a split-explicit time-integration method based on a 3rd order Runge-Kutta scheme (Skamarock et al., 2005; Wicker and Skamarock, 2002). Scalar transport is integrated with the Runge-Kutta scheme using 5th order (horizontal) and 3rd order (vertical) upwind-biased advection operators. Transported scalars include water vapor, the different hydrometeor categories and the chemical species. The cloud microphysics is described by the single moment (bulk water) approach (Lin et al., 1983). Mass mixing ratios of cloud water, rain, ice, snow, and graupel/hail are predicted. Cloud water and ice are monodispersed and rain, snow, and hail have prescribed inverse exponential size distributions. For the graupel/hail category, the intercept parameter of the exponential distribution is $4 \times 10^4 \text{ m}^{-4}$ and the density is 917 kg m^{-3} which corresponds to characteristics of hail particles.

The model includes both gas and aqueous phase chemistry representing O₃-NO_x-CH₄ chemistry (Barth et al., 2007a). The NO_x chemistry includes NO reaction with O₃, NO and O₃ formation from NO₂ photolysis, NO₂ reaction with OH to form nitric acid (HNO₃), and HNO₃ photolysis and OH oxidation to produce NO₂ and NO. Because NO and NO₂ have very low solubilities, their mixing ratios are not affected by the presence of liquid or ice hydrometeors. However, HNO₃ and other highly soluble species are readily scavenged by both liquid (via diffusion-limited mass transfer calculation) and ice (via the Langmuir equilibrium model approach, Tabazadeh et al., 1999; Popp et al., 2004) hydrometeors. Details of the algorithms are given in Barth et al. (2001, 2007a).

In addition to the chemically active species, a tracer of NO_x from lightning (LNO_x) is included in WRF. The LNO_x tracer corresponds to the NO mixing ratio produced by lightning flashes. The LNO_x tracer is transported only and does not undergo any chemical reactions.

3.2 The 10 July 1996 STERAO storm

The LNO_x production in the 10 July 1996 STERAO storm has been widely studied (Stith et al., 1999; Skamarock et al., 2003; Barthe et al., 2007b; Barth et al., 2007a,b). Different parameterizations and different models have been used to simulate this storm leading to a wide range of values for the production rate estimate. Large differences are found in LNO_x estimates that range from 36 moles per flash to 465 moles per *IC* flash (Barth et al., 2007b). Thus, it is interesting to investigate the origin of such discrepancies and to evaluate the uncertainties associated with each step of the LNO_x parameterization. The 10 July 1996 storm has also been chosen because there is a unique set of data for this storm: storm structure and kinematics from radar data, lightning flash characteristics and in-situ chemical species measurements from two aircraft (Dye et al., 2000).

During the STERAO-A experiment the ONERA VHF interferometric mapper (ITF) measured the total (*IC*+*CG*) lightning activity while the National Lightning Detection Network (NLDN) documented the *CG* activity (Dye et al., 2000). NLDN provided locations of the ground connections from the measurements of the electric and magnetic field due to the high current of return strokes (Cummins et al., 1998). ITF was designed to detect and locate VHF radiation emitted during both *IC* and *CG* flashes (Defer et al., 2001). VHF radiation is recorded during stepped leaders, dart leaders, recoil streamers and return strokes of negative *CG*s (Defer et al., 2001). Comparison between optical radiation detected by NASA Optical Transient Detector (OTD) and VHF radiation recorded by ITF for one passage over the STERAO-A domain (9 July 1996) showed consistent observations between OTD and ITF (Defer et al., 2006), suggesting that a flash sensed by OTD corresponds to a flash sensed by ITF. However, Boccippio et al. (2002) estimated the flash detection efficiencies to be 93% (nighttime) and 73% (local noon) for LIS and 56% (nighttime) and 44% (local noon) for OTD. Thus, extrapolations of the results reported here must be done cautiously as the detection of flashes by satellite instruments is less than that by the ITF system. Further, the 10 July 1996 STERAO storm is likely not a typical thunderstorm whose flash, physical structure, and dynamics characteristics are necessarily meaningful for extrapolation of LNO_x production to the global scale.

4 Control experiment

4.1 Initialization

The simulation performed is similar to those described by Skamarock et al. (2000, 2003) and Barth et al. (2001, 2007a). The environment was assumed to be homogeneous, thus a single profile was used for initialization. The initial profiles of the meteorological data were obtained from sonde and air-

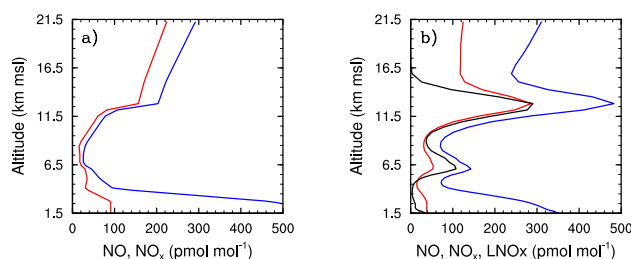


Fig. 2. Initial (a) and final (b) NO (red line) and NO_x (blue line) vertical profiles. The LNO_x tracer (black line at the final time of $t=180$ min) corresponds to the NO molecules produced by lightning flashes that are transported but do not chemically react. In (b), the mixing ratios are averaged over the model domain.

craft data (Skamarock et al., 2000). The convection was initiated with three warm (3°C perturbation) bubbles oriented in a NW to SE line. WRF is configured to a $160 \times 160 \times 20 \text{ km}^3$ domain with 161 grid points in each horizontal direction (1 km resolution) and 51 grid points in the vertical direction with a variable resolution beginning at 50 m at the surface and stretching to 1200 m at the top of the domain. The simulation was integrated at a 10 s time step. To keep the convection near the center of the model domain, the grid is moved at 1.5 m s^{-1} eastward and 5.5 m s^{-1} southward. The simulation was integrated for a 3-h period. While the observed storm lasted from 21:30 to 03:00 UTC, only the multicell and supercell stages are simulated. These stages correspond to 23:15–02:15 UTC in the observations.

Initial mixing ratios of the chemical species are the same as those in Barth et al. (2007a). Of interest to this study are NO, NO₂ and O₃ mixing ratios. NO and NO_x initial mixing ratios are relatively high near the surface, low in the mid-troposphere, and moderately high in the UTLS region (Fig. 2). O₃ mixing ratios are 60 ppbv near the surface and are fairly constant with height to 12 km m.s.l. where mixing ratios increase into the stratosphere. Because of the short integration time and small domain, there is very little effect of lightning-produced NO on O₃ mixing ratios in these simulations. The initiation process is the same in all the simulations.

The details of the control experiment (REF) are summarized in Table 1. The total flash rate is computed from the non-precipitation and precipitation ice mass flux product. The cloud-to-ground flash rate is considered null throughout the simulation since very few *CG* flashes were observed in this storm (83 *CG* flashes of both polarities and 5428 total flashes between 21:52 and 03:00 UTC). The lower and upper modes of the bimodal distribution correspond to the -15°C and the -50°C isotherms, respectively. The flash length of an individual storm is assumed to be lognormal in the range 1 to 400 km (Defer et al., 2003). As in the observations (Defer et al., 2001, 2003), the percentage of the short flashes (<1 km) is set to 47%. Among these short flashes, 36% are

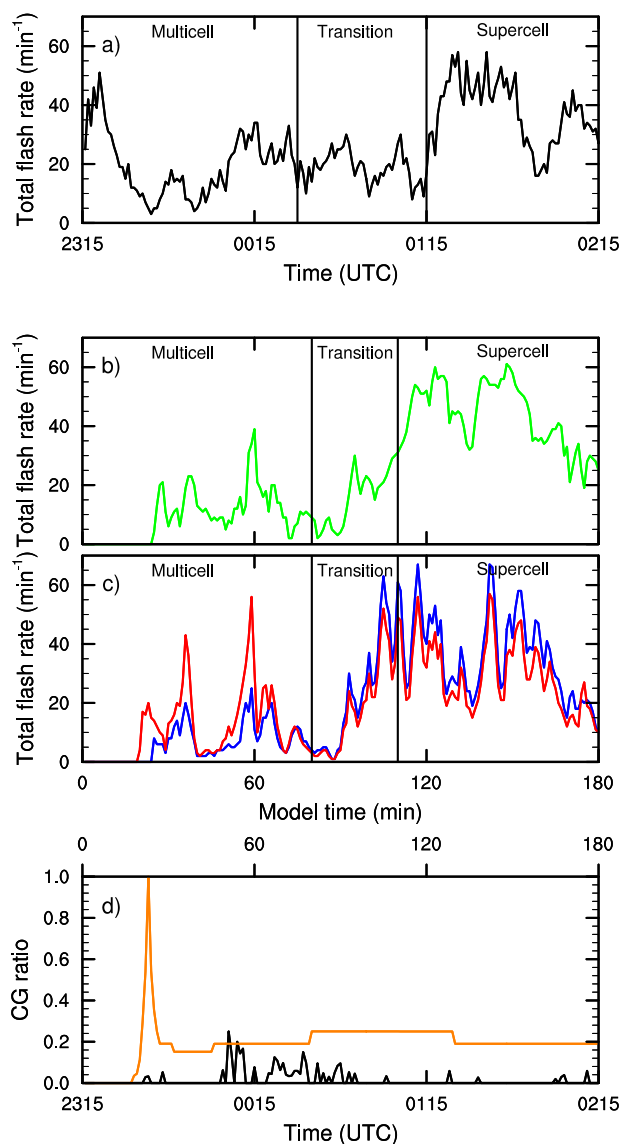


Fig. 3. Temporal evolution of the total flash rate (a) from observations (black curve), (b) from the non-precipitation and precipitation ice mass flux product (green curve), and (c) from Price and Rind (1992) in the entire convective system (blue curve) and from Price and Rind (1992) in each individual cells (red curve). The different stages of the storm are indicated both for the observed storm (a) and for the simulated storm (b and c). The CG ratio from observations (black curve) and from the Price and Rind (1993) parameterization (orange curve) is also plotted (d).

considered as short duration flashes (<1 ms). In this simulation, it is assumed that the short duration flashes produce as much NO molecules per flash length as a normal short flash. The production rate of NO per flash depends on the flash length and on the pressure. The original a and b parameters

of Wang et al. (1998) from laboratory studies have been multiplied by 5 to best match with observations ($a_{\text{REF}}=1.7 \times 10^{21}$ and $b_{\text{REF}}=6.5 \times 10^{16}$).

4.2 Results

The dynamics and the microphysics structure of this storm has been studied previously (Skamarock et al., 2000, BDB07). These studies showed that the WRF simulations compare well to the radar data. Based on the storm structure and dynamics, three different stages have been identified in this storm: a multicell (0–80 min corresponding to 23:15–00:30 UTC), a transition (80–110 min corresponding to 00:30–01:05 UTC) and a supercell (110–180 min corresponding to 01:05–02:30 UTC). For comparison of observations to the model results, the number of observed lightning flashes are reported for the period 23:40 to 02:15 UTC.

First, the flash rate computed from the ice mass fluxes is compared to observations. The simulated and observed total flash rates are shown in Fig. 3a and b. The number of flashes observed between 23:40 and 02:15 UTC was 3728, while that simulated was 4253 flashes for the 3-h simulation. The first simulated flash occurs after 25 min of simulation. In the multicell stage, several cells are at different evolution stages, so the extreme values and the average values of the flash rate are compared. The minimum and maximum values in the REF simulation are 2 and 39 fl. min⁻¹, respectively, which is similar to the minimum and maximum observed values (3 and 34 fl. min⁻¹; Table 3). The mean flash rate during the multicell stage is 9.2 fl. min⁻¹ for the simulated flash rate, which is similar to the 10.5 fl. min⁻¹ observed. During the transition stage, the ice mass flux parameterization underestimates the mean flash rate (15.7 vs. 20.4 fl. min⁻¹) and overestimates it in the supercellular stage (43.8 vs. 33.8 fl. min⁻¹). BDB07 have shown that the supercellular stage begins ~20 min earlier in the simulation compared to observations and the simulated mass flux product is ~20 times larger than observed in this stage of the storm. The differences in the simulated and observed microphysics and dynamics features cause the differences in the observed and simulated flash rate.

Figure 4 shows horizontal and vertical cross sections of the simulated NO mixing ratio during the different stages of the storm. During the multicell stage, NO production by lightning occurs mainly in the convective cores. At 3600 s (Fig. 4a), five different cells are present in the domain: three of them are located along a NW-SE axis as initialized and the two others are on the eastern side of the NW and middle cells. Peaks of NO up to 3000 pmol mol⁻¹ are collocated with the cells. NO mixing ratios higher than 1000 pmol mol⁻¹ are related to fresh production of NO by lightning flashes. Downwind of the convective cores (SE of the storm cores), NO values lower than 1000 pmol mol⁻¹ are due to the transport and dilution of NO produced by lightning earlier in the simulation. Figure 4b shows that high values of the NO mixing ratio are mainly located in the range 6–7.5 km altitude and

Table 1. Summary of the sensitivity tests. *CG* ratio is the fraction of total flashes that are cloud-to-ground. MF: derived from the non-precipitation and precipitation ice mass flux product; Obs.: Observations; PR92: Price and Rind (1992) for the global system; PR92/cell: Price and Rind (1992) in each individual cell; Cst: constant; LN: lognormal distribution; SDF: short duration flashes; DC00/–/–: bimodal distribution from DeCaria et al. (2000)/lower isotherm (°C)/upper isotherm (°C); P_{IC} : production rate per meter of *IC* flash; P_{CG} : production rate per meter of *CG* flash; *W*: a and b parameters from Wang et al. (1998).

Name of the experiment	Total flash rate	<i>CG</i> ratio	Flash length	SDF	Cell identification	Horizontal distribution	Vertical distribution	Production rate per flash length
REF	MF	0	LN	yes	yes	random	DC00/–15/–50	$P_{IC}=P_{CG}=W \times 5$
FR_OBS	Obs.	Obs.	LN	yes	yes	random	DC00/–15/–50	$P_{IC}=P_{CG}=W \times 5$
FR_PR92	PR92	0	LN	yes	yes	random	DC00/–15/–50	$P_{IC}=P_{CG}=W \times 5$
FR_PR92_CELL	PR92/cell	0	LN	yes	yes	random	DC00/–15/–50	$P_{IC}=P_{CG}=W \times 5$
CG_CST	MF	Cst	LN	yes	yes	random	DC00/–15/–50	$P_{IC}=P_{CG}=W \times 5$
CG_OBS	MF	Obs.	LN	yes	yes	random	DC00/–15/–50	$P_{IC}=P_{CG}=W \times 5$
CG_PR93	MF	PR93	LN	yes	yes	random	DC00/–15/–50	$P_{IC}=P_{CG}=W \times 5$
ISO_UP_45	MF	0	LN	yes	yes	random	DC00/–15/–45	$P_{IC}=P_{CG}=W \times 5$
ISO_LOW_20	MF	0	LN	yes	yes	random	DC00/–20/–50	$P_{IC}=P_{CG}=W \times 5$
LENGTH_21	MF	0	21 km	no	yes	random	DC00/–15/–50	$P_{IC}=P_{CG}=W \times 5$
NO_SDF	MF	0	LN	no	yes	random	DC00/–15/–50	$P_{IC}=P_{CG}=W \times 5$
VOL_20_DC	MF	0	21 km	no	yes	20 dBZ	DC00/–15/–50	$P_{IC}=P_{CG}=W \times 5$
VOL_20	MF	0	21 km	no	yes	20 dBZ	uniform	$P_{IC}=P_{CG}=W \times 5$
VOL_CLD	MF	0	21 km	no	yes	cloud	uniform	$P_{IC}=P_{CG}=W \times 5$
VOL_ALLCLD	MF	0	21 km	no	no	cloud	uniform	$P_{IC}=P_{CG}=W \times 5$
WANG_10	MF	0	LN	yes	yes	random	DC00/–15/–50	$P_{IC}=P_{CG}=W \times 10$
WANG_1	MF	0	LN	yes	yes	random	DC00/–15/–50	$P_{IC}=P_{CG}=W$
PROD.CG_2	MF	Obs.	LN	yes	yes	random	DC00/–15/–50	$P_{IC}=P_{CG}/2=W \times 5$
PROD.CG_10	MF	Obs.	LN	yes	yes	random	DC00/–15/–50	$P_{IC}=P_{CG}/10=W \times 5$

11–14 km altitude due to the bimodal distribution of the flash segments.

At 5400 s, during the transition stage, the flash rate is lower than in the multicell stage (see Fig. 3) which can explain why peak NO values decrease (Fig. 4c). NO starts to spread over a large region in the anvil. The vertical cross section during the transition stage (Fig. 4d) confirms that less LNO_x is produced at this time of the simulation.

In the supercell stage ($t=7200$ s), the flash rate (Table 3) is higher than in the two other stages with values in the range 19–61 fl. min^{–1} leading to high values of the NO mixing ratio. In the anvil, values higher than 4000 pmol mol^{–1} extend horizontally for 25 km from the convective core. NO mixing ratios up to 1000 pmol mol^{–1} can be found 100 km downwind of the updraft maximum. Even though the LNO_x parameterization produces LNO_x only in a small region in and downwind of the convective core, NO molecules are transported and diluted in the whole cloud. Lightning flashes are then responsible for a large amount of NO in the whole system during the supercell stage (Fig. 4f).

The NO mixing ratios from the model are next compared to the University of North Dakota's (UND) Citation aircraft measurements. The observed NO vertical cross-section (Fig. 5 "Observations") is a result of projecting the NO air-

craft measurements collected between 23:16 and 00:36 UTC onto the across-anvil plane, which is ~60 km downwind of the convective core. Several regions of simulated NO mixing ratio higher than 540 pmol mol^{–1} can be seen at the altitude of 11.5 km and up to 13 km which is in agreement with observations (Fig. 5 "REF").

NO transects across the anvil during the multicell and the transition stage of the storm have been plotted in Fig. 6. After 1 h of simulation (left panels), the transect is 10 km downwind of the southeastern cell. The simulated transect REF compares well with observations. A peak of 1800 pmol mol^{–1} is simulated and NO > 500 pmol mol^{–1} extends over a distance of 20 km in the simulation. The distance over which the observed NO mixing ratio is higher than 500 pmol mol^{–1} is 30 km. Thus, WRF with its new LNO_x parameterization is able to simulate peaks of NO higher than 1000 pmol mol^{–1} in the region where lightning flashes are mostly triggered and propagate. After 1 h 30 min of simulation (right panels), the transect is located 50 km downwind of the main convective core. The trends of the simulated and observed transects are the same, however the simulated values are lower in magnitude compared to the observations. The lightning activity in this storm started at 21:52 UTC, i.e. 108 min before the first flash was triggered in the simulation

Table 2. Summary of the sensitivity tests results. For the NO_SDF experiment, the number in parentheses corresponds to the number of NO moles produced per flash that is not a short duration flash. For the NO peak value column, the numbers in brackets represent the NO peak value in the three different stages (multicell/transition/supercell) of this storm. Observations are values analyzed from observations by Skamarock et al. (2003).

	Average NO moles per flash (moles)	NO peak value (nmol mol ⁻¹)	NO _x flux through the anvil (10 ⁻⁸ mol m ⁻² s ⁻¹)	Total amount of LNO _x produced for the life of the storm (kg(N))
Observations	43.2		5.8	32–88 × 10 ²
REF	121.3	14.2 (13.8/5.2/14.2)	5.72 ± 1.70	72.22 × 10 ²
FR_OBS	126.3	16.7 (9.4/7.4/16.7)	6.50 ± 2.02	66.67 × 10 ²
FR_PR92	119.6	15.2 (4.2/9.0/15.2)	4.46 ± 1.17	61.73 × 10 ²
FR_PR92_CELL	121.0	12.5 (7.3/9.3/12.5)	6.84 ± 2.78	59.14 × 10 ²
CG_CST	121.1	19.6 (9.3/7.8/19.6)	5.79 ± 2.68	72.13 × 10 ²
CG_OBS	122.6	23.6 (8.1/5.1/23.6)	5.86 ± 1.94	72.99 × 10 ²
CG_PR93	124.5	24.1 (9.7/8.5/24.1)	5.59 ± 2.02	74.16 × 10 ²
ISO_UP_45	122.3	21.9 (8.2/7.8/21.9)	6.75 ± 3.00	72.81 × 10 ²
ISO_LOW_20	127.0	17.0 (7.2/6.5/17.0)	6.10 ± 2.21	75.62 × 10 ²
LENGTH_21	125.0	19.5 (7.4/5.6/19.6)	5.45 ± 1.79	74.45 × 10 ²
NO_SDF	120.6 (146.2)	16.9 (9.3/8.5/16.9)	5.75 ± 2.00	71.85 × 10 ²
VOL_20_DC	114.4	3.5 (1.5/1.3/3.5)	8.51 ± 3.17	68.16 × 10 ²
VOL_20	131.9	4.9 (1.9/2.1/4.9)	12.66 ± 5.62	78.53 × 10 ²
VOL_CLD	126.2	2.5 (1.2/1.4/2.5)	15.21 ± 7.66	75.15 × 10 ²
VOL_ALLCLD	123.0	1.8 (0.5/0.9/1.8)	15.12 ± 3.22	73.23 × 10 ²
WANG_10	245.7	29.6 (27.4/10.6/29.6)	9.65 ± 3.32	146.31 × 10 ²
WANG_1	24.6	2.9 (2.9/1.1/2.9)	2.62 ± 0.42	14.63 × 10 ²
PROD_CG_2	123.1	21.4 (6.5/5.4/21.4)	5.89 ± 1.96	70.20 × 10 ²
PROD_CG_10	129.2	21.6 (9.3/5.4/21.6)	6.14 ± 2.08	76.93 × 10 ²

Table 3. Total number of flashes, mean flash rate and peak values of the flash rate for each stage of the storm and for the entire storm (All). M, T and S correspond to the multicell, the transition and the supercell stages, respectively. The time intervals for computing the number of flashes in the transition and supercell stages of the storm are displayed in Fig. 3. For the observed multicell stage, the time interval is from 23:40 to 00:30 UTC.

Experiment	Total number of flashes				Average flash rate and standard deviation (min ⁻¹)				Extreme values (min ⁻¹)		
	M	T	S	All	M	T	S	All	M	T	S
FR_OBS	784	918	2026	3728	10.5 ± 8.1	20.4 ± 5.5	33.8 ± 14.1	23.9 ± 13.1	3–34	9–30	8–58
REF	728	456	3069	4253	9.2 ± 7.2	15.7 ± 9.6	43.8 ± 11.0	27.3 ± 17.4	2–39	2–30	19–61
FR_PR92	487	706	2494	3687	8.9 ± 5.5	23.5 ± 19.3	35.6 ± 13.9	23.6 ± 17.7	2–25	1–63	10–67
FR_PR92_CELL	874	574	2042	3490	14.6 ± 11.7	19.1 ± 16.0	29.2 ± 11.5	21.9 ± 14.2	2–56	1–52	18–57

(25 min after the beginning of the simulation or 23:40 UTC). NO may have accumulated in the environment of the storm leading to larger values than simulated. In summary, the WRF model coupled with the new LNO_x scheme gives results in good agreement with observations both near the convective cores and in the anvil.

The effect of the transport and lightning production of NO can be seen by comparing NO and NO_x final mixing ratios with their initial values. Figure 2 shows the NO, NO_x and LNO_x (a tracer of NO produced from lightning) vertical profiles horizontally-averaged over the model domain after 3 h of simulation. The NO and NO_x vertical profiles are impacted by transport, chemistry processes and light-

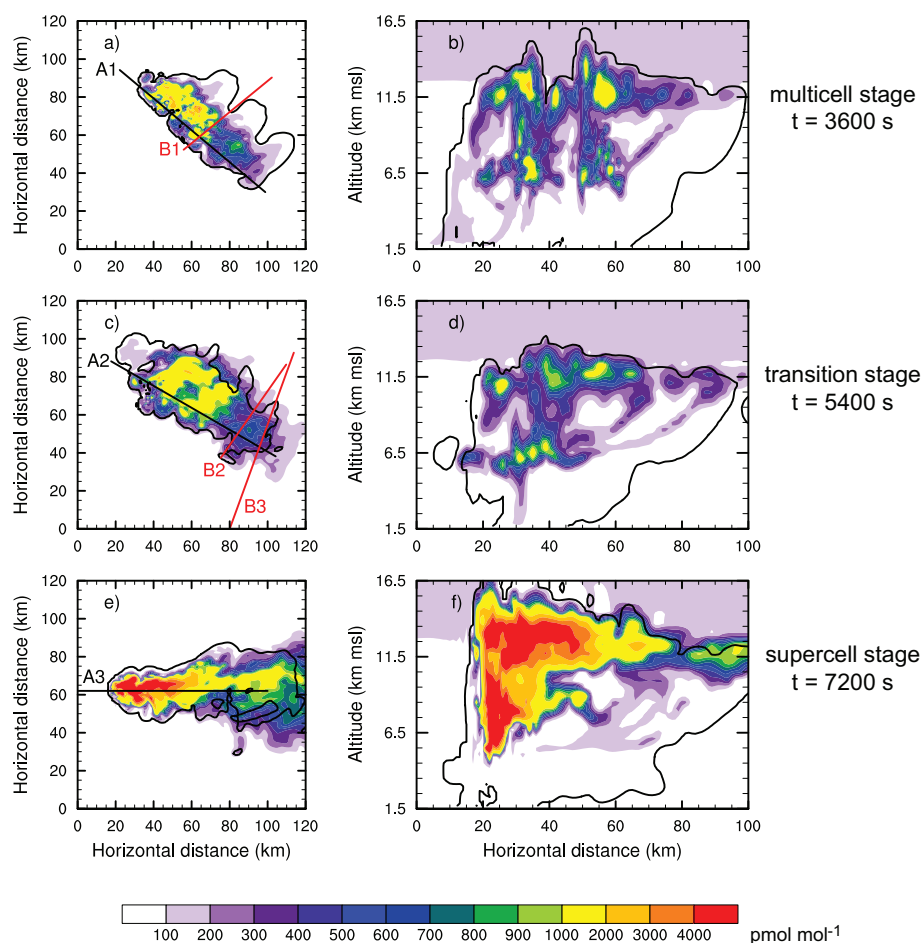


Fig. 4. NO mixing ratio (in pmol mol^{-1}) at 11.5 km m.s.l. (left column) and vertical cross sections along the anvil axis (right column). The results are shown during the multicell ($t=3600$ s; top row), the transition ($t=5400$ s; middle row) and the supercell ($t=7200$ s; bottom row) stages. Results are for the reference simulation (REF). The black line segments A1, A2 and A3 correspond to the location of the vertical cross sections. The red line segments B1, B2 and B3 correspond to the transects across the anvil 10 km downwind of the convective core at $t=3600$ s (Figs. 6 and 7, left columns), to the transect across the anvil 50 km downwind of the convective core at $t=5400$ s (Figs. 6 and 7, right columns) and to the transect across the anvil 60 km downwind of the convective core at $t=6000$ s (Fig. 5), respectively.

ning flashes. The NO_x in the boundary layer is transported to the mid- and upper troposphere by the updraft; approximately 45% of the anvil air is from air that was entrained into the storm (Barth et al., 2007a). The NO_x mixing ratio at the ground is reduced from $600 \text{ pmol mol}^{-1}$ (Fig. 2a) to $350 \text{ pmol mol}^{-1}$ (Fig. 2b) due to the chemistry converting NO_x to HNO₃. When comparing the NO and LNO_x curves, it can be seen that the two peaks at 13.0 km m.s.l. and 6.5 km m.s.l. are caused by NO production by lightning flashes. The intense vertical motions and the high electrical activity in the 10 July 1996 STERAO storm causes the modeled NO mixing ratio to increase by 120% at 13 km m.s.l. and by 400% at 6.5 km m.s.l.

The simulated NO_x flux through the anvil is $5.72 \times 10^{-8} \text{ moles m}^{-2} \text{ s}^{-1}$, which is similar to the value derived from observations reported by Skamarock et al. (2003)

of $5.8 \times 10^{-8} \text{ moles m}^{-2} \text{ s}^{-1}$ (Table 2). In this simulation, a typical flash is 21.7 km long. The mean production rate per flash calculated by dividing the total production of NO by the total number of flashes is 121.3 moles of NO (7.3×10^{25} molecules NO). This production rate is in the lower range of the estimates from the last 5 years as reported by Schumann and Huntrieser (2007). Furthermore, our estimate is lower than most of the 3-D CRM studies.

5 Sensitivity analyses

To examine the key processes in the LNO_x parameterization for CRMs, the sensitivity of the NO mixing ratio to several parameters is investigated. In particular, the impact of the total flash rate (Sect. 5.1), the CG rate (Sect. 5.2), the altitudes

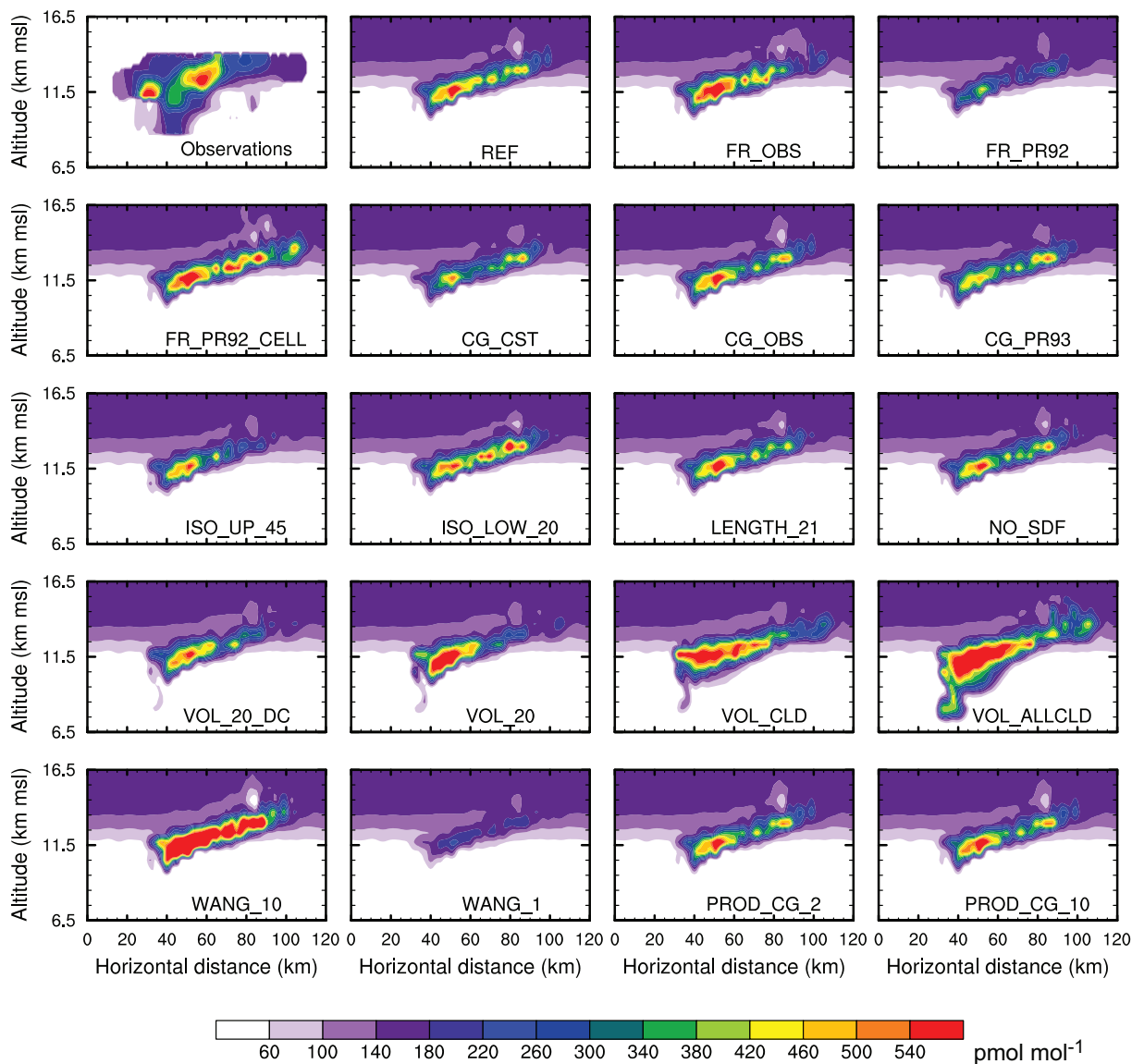


Fig. 5. Vertical cross sections 60 km downwind of the convective core of the NO mixing ratio (pmol mol^{-1}) across the anvil at 6000 s. Observations are a composite from airborne measurements between 23:16 and 00:36 UTC (from Skamarock et al., 2003). The location of the transect B3 is shown on Fig. 4. The different simulations are defined in Table 1.

of the peaks of the NO source (Sect. 5.3), the flash length (Sect. 5.4), the short duration flashes (Sect. 5.5), the spatial distribution of the NO molecules (Sect. 5.6), and the NO production rate per flash (Sect. 5.7) are studied. A summary of the name and conditions of the experiments is given in Table 1.

5.1 Total flash rate

When simulating the production of LNO_x in thunderstorms, the total flash rate is fundamental. Two different parameterizations for the total flash rate have been tested in this section

and compared to observations from the ONERA interferometer (Defer et al., 2001). First, the total flash rate can be deduced from the non-precipitation and precipitation ice mass flux product as described in Sect. 2 (Eq. 1) and used in the REF simulation. Secondly, a sensitivity simulation is performed using the flash data from the ONERA interferometer (FR_OBS, Table 1). To determine the flash rate in each convective cell i , the cell flash rate ($F^{(i)}$) is assumed to be in proportion to the cell ice mass flux product ($f^{(i)}$). That is,

$$F^{(i)} = F \times \frac{f^{(i)}}{\sum_{(i)} f^{(i)}} \quad (3)$$

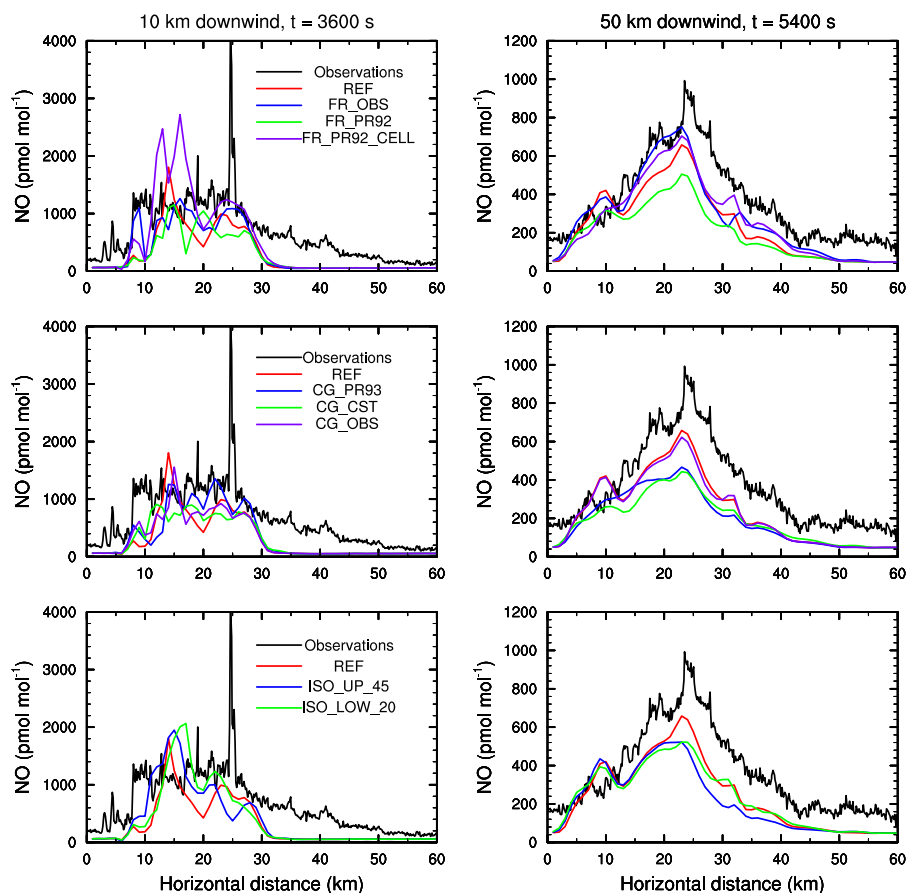


Fig. 6. NO (pmol mol^{-1}) transects across the anvil during the multicell stage ($t=3600$ s) at 11.6 km m.s.l. and 10 km downwind of the southeastern cell (left column) and during the transition stage ($t=5400$ s) at 11.2 km m.s.l. and 50 km downwind of the main convective core (right column). The locations of the transects B1 and B2 are shown on Fig. 4. The different simulations are defined in Table 1.

where F is the total flash rate. Thirdly, the total flash rate can be determined from the maximum vertical velocity w_{\max} (m s^{-1}) following Price and Rind (1992):

$$F_{PR} = 5.7 \times 10^{-6} \times w_{\max}^{4.5} \quad (4)$$

Two different simulations use the Price and Rind (1992) approach for the flash rate. In the first simulation, w_{\max} is the maximum vertical velocity in the whole domain: the total flash rate is then computed for the whole domain (FR_PR92). The distribution of the flash rate in each cell is in proportion to the cell ice mass flux product (Eq. 3). Because the Price and Rind (1992) parameterization has been used several times in CRMs (Pickering et al., 1998; Fehr et al., 2004; Barth et al., 2007b) where several cells can be identified, a second simulation in which the total flash rate per cell is computed from the maximum vertical velocity in each individual cell (FR_PR92_CELL) is performed. That is, Eq. (4) is applied for each cell. Equation (4) has been rescaled for the FR_PR92 and FR_PR92_CELL simulations in order to best match with observations. For FR_PR92 and

FR_PR92_CELL, Eq. (4) is multiplied by 0.19 and 0.16, respectively, to have approximately the same total number of flashes as observed.

The simulated total flash rate is compared to that predicted by the ice mass flux product and to the observed flash rate. In the REF and FR_PR92 simulations, the first flash is triggered at 25 min while the lightning activity starts at 19 min in FR_PR92_CELL, i.e. only 3 min after ice particles start to form in this simulated storm. However, the cloud becomes electrified after charges are exchanged during collision between more or less rimed ice particles (e.g. Takahashi, 1978; Jayaratne et al., 1983; Saunders et al., 1991). Using an explicit electrical scheme in a CRM, Barthe and Pinty (2007b) showed that the first flash was triggered 20 min after ice particles appeared in the cloud. Since the maximum vertical velocity in their simulated storm did not exceed 20 m s^{-1} , a shorter delay can be expected in the 10 July storm which is more intense. The simulated 10 July STERAO storm starts to produce ice particles at 16 min and the flux hypothesis allows the first flash to be triggered at 25 min, i.e. 9 min later. In the

FR_OBS simulation, the observed flash rate is available since 21:52 UTC, but it is only taken into account starting at 25 min (23:40 UTC) to allow the cloud to develop, to electrify and to trigger lightning.

As some differences exist between the time of the observed and simulated stages of this storm, the lightning activity is compared in each stage. Table 3 shows highly variable results for FR_PR92 and FR_PR92_CELL. An important point is that the flash rate in FR_PR92 and FR_PR92_CELL is in advance compared to REF and to observations (Fig. 3). For example, at the end of the transition stage the total flash rates in the FR_PR92 and FR_PR92_CELL simulations increase 10 min before the REF simulation and the observed flash rate increase. In the Price and Rind (1992) parameterization for the total flash rate, only the maximum vertical velocity is considered. There is no information about the ice content or about conditions favorable for the non-inductive separation mechanism which can lead to this lag. Thus, contrary to the total flash rate deduced from the flux hypothesis, the total flash rate from Price and Rind (1992) seems to be not as suitable for use in CRM as it does not take into account the microphysical development of the storm which is of primary importance for the cloud electrification. Using an explicit electrical scheme to simulate a STEPS supercellular storm, Kuhlman et al. (2005) concluded that there is no linear correlation between the maximum vertical velocity and the total flash rate. Deierling (2006) confirmed this conclusion using radar and lightning data.

To examine the effect of using different flash rate parameterizations, the NO mixing ratio downwind of the convective core is analyzed. Figure 5 shows the vertical cross sections of the NO mixing ratio across the anvil at 6000 s. The REF, FR_OBS and FR_PR92_CELL simulations display similar results having several spots in the anvil with NO mixing ratio >500 pmol mol⁻¹. The lower values of the NO mixing ratio in the anvil for the FR_PR92 simulation are not due to the lower flash rate during the transition stage (Fig. 3) since 1193 flashes are produced in FR_PR92 and 1184 in REF, but instead are attributed to the lower flash rate during the multicell stage (487 flashes in FR_PR92 and 728 flashes in REF). Indeed, NO molecules are produced mostly near the convective core and it takes ~40 min to be transported in the anvil to 50 km downwind. Because the number of flashes in the multicell stage is higher for FR_OBS and FR_PR92_CELL than for the REF simulation, the NO mixing ratios for FR_OBS and FR_PR92_CELL are also higher than those for REF in the vertical cross section at 6000 s. In most cases, the simulations producing more LNO_x near the convective core (transect 10 km downwind at 3600 s) are the ones that have more NO transported in the anvil (transect 50 km downwind at 5400 s).

The NO_x flux through the anvil varies from $4.46 \times 10^{-8} \text{ mol m}^{-2} \text{ s}^{-1}$ for FR_PR92 to $6.84 \times 10^{-8} \text{ mol m}^{-2} \text{ s}^{-1}$ for FR_PR92_CELL (Table 2). As with the NO mixing ratios 50 km downwind of the

convective cells, the NO_x flux depends on the lightning flash rate during the multicell stage of the storm because of the >40 min of transport time from the convective cells to the location of the flux calculation. An increase of 79% in the flash rate is related to an increase of 53% in the NO_x flux through the anvil. The non-linear change between changes in flash rate and NO_x flux from these two simulations is due to the placement of the flashes and therefore the placement of the NO source. The FR_PR92_CELL simulation distributes the NO source according to w_{max} in the individual cells, while the FR_PR92 simulation distributes the NO source according to the ice mass flux product (Eq. 3). These locations may be similar but not necessarily exactly the same.

5.2 Cloud-to-ground flash rate

Boccippio et al. (2001) analyzed four years of OTD and NLDN flash rate data over the United States and found that the CG to IC ratio may be dominated by storm type, morphology, and level of organization instead of environmental parameters. Here, we examine the influence of the CG to IC ratio on the NO mixing ratios. In this study, the cloud-to-ground ratio α is defined by:

$$\alpha = \frac{N_{CG}}{N_{IC} + N_{CG}} \quad (5)$$

Price and Rind (1993) estimated the cloud-to-ground ratio α_{PR} from the depth Z of the layer from the freezing layer to the cloud top (simulation CG_PR93).

$$\alpha_{PR} = \frac{1}{1 + \beta} \quad (6)$$

with:

$$\begin{aligned} \beta &= \frac{N_{IC}}{N_{CG}} \\ &= 0.021Z^4 - 0.648Z^3 + 7.493Z^2 - 36.54Z + 63.09 \quad (7) \end{aligned}$$

N_{IC} and N_{CG} are the number of IC and CG flashes, respectively. The cloud top height is computed taking the average altitude where the total hydrometeor mixing ratio decreases to $10^{-5} \text{ kg kg}^{-1}$. Two other simulations (Table 1) have been performed with the observed α_{OBS} ratio (CG_OBS), and with a constant value (CG_CST). The constant value is $\alpha_{\text{CST}}=0.02$ which corresponds to α_{OBS} averaged during the simulated storm. These simulations are compared to REF in which CG flashes are not considered.

Figure 3 displays the observed and simulated $N_{CG}/(N_{IC}+N_{CG})$ ratio. The α_{PR} ratio from Price and Rind (1993) reaches 1 as soon as the electrical activity begins, when Z equals 4850 m. Then, as the storm is developing and extending vertically, the α_{PR} ratio decreases rapidly to values ~0.2. This value is 10 times larger than the mean α (0.018) deduced from observations between 23:15 and 02:15 UTC. Even when the observed convection started,

α_{OBS} did not reach such high values. Lang et al. (2000) studied this anomalously low *CG* rate in two STERAO storms and concluded that it could originate from an elevated charge region (MacGorman et al., 1989). MacGorman et al. (1989) hypothesized that strong updrafts can suspend the negative charge center to higher altitudes than in ordinary storms. This elevated charge would favor *IC* flashes over *CG* flashes. Here, we can investigate the impact of the high α ratio on the LNO_x production compared to the other simulations.

Pickering et al. (1998) used Eq. (7) to estimate the *CG* ratio in seven different storms. In the two mid-latitude continental events in which *CG* flash data were available, the simulated *CG* rate was in reasonable agreement with observations. For the total flash rate in the simulated 21 July 1998 EULINOX storm, Fehr et al. (2004) rescaled Eq. (7) by a factor of 1.10. As for the total flash rate estimated by the Price and Rind (1992) parameterization, it is not clear if Eq. (7) needs to be rescaled depending on the storm or on the model. More tests should be done on several convective cases with the same model and with available observations.

When comparing the NO mixing ratios along the transects and in the vertical cross section across the anvil (Figs. 5 and 6), the *CG*.OBS results are in better agreement with the REF simulation and with observations than *CG*.PR93 and *CG*.CST results. The *CG*.PR93 and *CG*.CST results have NO mixing ratios lower than the observations both near the convective region and in the anvil. Consequently, it is important to have the right number and temporal distribution for the *CG* flashes. Because the α_{PR} ratio is ~ 10 times greater than α_{OBS} , more NO is produced in the mid troposphere at the expense of the upper troposphere resulting in a 33% increase of NO in the mid-troposphere and a 20% decrease in the upper troposphere (Fig. 8). However, even if the NO mixing ratio is low compared to the reference run and to the observations, it reaches 1000 pmol mol⁻¹ in the transects 10 km downwind.

Despite an increase in the *CG* rate by a factor 10 between *CG*.CST and *CG*.PR93 (the total number of flashes being constant), NO produced by lightning is not significantly impacted. It causes a decrease of 3.5% in the flux through the anvil and an increase of 2.8% in the total amount of nitrogen produced during the storm lifetime. The flux through the anvil is decreased when there are more *CG* flashes because even if more NO molecules are produced, they are produced at lower altitudes and it takes more time to be transported in the anvil.

5.3 Altitude of the upper and lower modes for the bimodal distribution

Typically the *IC* discharge has a bilevel structure (Shao and Krehbiel, 1996), which is correlated with the main negative and upper positive charge regions of the storm. Rison et al. (1999), Thomas et al. (2001) and Krehbiel et al. (2000) deduced from the use of the Lightning Mapping Array in

New Mexico and Oklahoma that the main negative charge is located in the middle level at 5–6 km m.s.l. while the upper positive charge is centered at about 10–12 km altitude. By examining electric field soundings in different thunderstorms, Stolzenburg et al. (1998) found that the temperature at the center of the main negative charge region varies from -4°C to -32°C with a mean value of -15.7°C . Thus, the production of NO_x and its subsequent distribution by updrafts and downdrafts may be sensitive to the altitudes chosen for the bimodal distribution.

Two sensitivity tests have been performed to investigate the impact of a change in the altitude of the two levels where flash segments are preferentially distributed on the LNO_x mixing ratio and budget. First, the upper isotherm is set to -45°C (simulation ISO_UP_45) instead of -50°C in the REF simulation. Second, the lower isotherm is set to -20°C (ISO_LOW_20) instead of -15°C in REF to account for the hypothesized elevated charge mechanism in this storm (Lang et al., 2000).

Using the -45°C isotherm as the upper level for the flash segments distribution mainly shifts the LNO_x production in the upper troposphere to the altitude of 11.5 km m.s.l. instead of the 12 km m.s.l. Near the convective core and slightly downwind, the NO mixing ratio is fairly similar in the REF, ISO_UP_45 and ISO_LOW_20 simulations (Fig. 6). The LNO_x produced in the lower mode for ISO_LOW_20 is more readily transported to high altitudes than in the REF simulation.

The impact of moving the altitude of the upper and lower modes in the vertical distribution of the flash segments has an impact on the flux of NO_x through the anvil (Table 2). Lowering the upper mode and raising the lower mode both result in an increase of the NO_x flux through the anvil. DeCaria et al. (2000) tested different temperatures (-40°C and -30°C) for the upper isotherm of their bimodal distribution in the 12 July 1996 STERAO storm. They found that by lowering the upper mode of the flash distribution the maximum of the NO plume occurs at a lower altitude.

5.4 Flash length

Previous studies have estimated the flash length to be in the range 20–50 km (Théry et al., 2000). For the 10 July 1996 STERAO storm analysis, Defer et al. (2001) have shown that the flash length in this storm is not constant and varies from 0.02 and 474 km. They have concluded that the average value of the flash length is 19 km but is 34 km if short duration flashes (flashes < 1 ms) are not considered. Pinty and Barthe (2008) conducted an ensemble of simulations of two idealized electrified storms with a cloud-resolving model coupled to an explicit electrical scheme. They showed that the number of segments in an individual flash is highly variable from flash to flash but looks like a lognormal distribution.

To explore the importance of the variation of the flash length distribution on the production of NO from lightning,

a simulation is performed using a constant flash length of 21 km (LENGTH_21, Table 1). The objective of this sensitivity test is to determine whether a detailed description of the flash length distribution (e.g. the lognormal distribution) is needed to correctly represent the LNO_x production or whether a constant flash length is sufficient. The value of 21 km corresponds to the mean flash length simulated when a lognormal distribution for the flash length is used and when short duration flashes are taken into account.

Using the more realistic lognormal distribution for the flash length (REF) leads to results fairly similar to a constant value (LENGTH_21) near the convective core and downwind. The main difference arises in Fig. 8 where the LENGTH_21 and REF profiles differ between 5.5 and 10.5 km m.s.l. These mean profiles show that LENGTH_21 tends to produce more NO molecules in the lower part of the cloud. This difference can be due to the treatment of the short flashes <1 km since they are made up of only one grid point. Due to the bimodal vertical distribution that is used, the short flashes tend to be produced in the upper part of the cloud (~12 km m.s.l.). This is slightly higher than the analysis of Defer et al. (2001) who showed that the VHF sources with strong radiation were mostly located in altitude between 7.5 and 10.5 km m.s.l. The increase of sources at lower altitude increases the NO production per flash from 121.3 moles fl.⁻¹ in REF to 125.0 moles fl.⁻¹ in LENGTH_21 (=3.1%) because of the pressure dependence in the NO production (Eq. 2).

Additional analysis and sensitivity tests showed if the same number of NO molecules are produced per meter of flash for all the flashes, that the flashes >30 km are responsible for nearly 80% of the lightning-produced NO while these longer flashes were only ~30% of the number of flashes. Flashes <1 km in length represented 46% of the total number of flashes, but produced only 2% of the lightning-generated NO. When a constant flash length of 34 km instead of 21 km is assumed, the produced NO mixing ratio increases linearly. In this case, a 62% increase of the flash length results in a 63% increase of the NO mixing ratio everywhere in the domain (not shown).

5.5 Short duration flashes

In the 10 July 1996 STERAO storm, Defer et al. (2001) defined the short duration flashes as discharges lasting less than 1 ms while the mean flash duration is 240 ms in this storm. They reported that between 22:50 and 23:30 UTC up to 45% of the recorded flashes were short duration flashes.

Analyzing data from the lightning mapping array, Harlin et al. (2003) identified three different types of short duration flashes lasting less than 80 ms: the isolated events, the precursor events, and the high source power events. Several studies have shown that taking into account or not the short duration flashes does not modify the flash rate trend but can significantly change its magnitude (Lang et al., 2000; Wiens et al., 2005). Whether these short duration flashes should be

considered or not as part of the total lightning flash rate and as a source of nitrogen oxides is a matter of debate.

To investigate the possible impact of short duration flashes in the LNO_x production, a sensitivity simulation (NO_SDF) has been performed. In this simulation, the lognormal distribution is used but it is hypothesized that the short duration flashes do not produce NO molecules. It is worth recalling that the reference run (REF) assumes that short duration flashes produce as many NO molecules per meter of flash as “normal” flashes. It is assumed that the flash length of a short duration flash is 1 km, and that 36% of the flashes that are 1 km in length are short duration flashes.

In the NO_SDF simulation 4253 flashes have been triggered among which 699 were short duration flashes. If short duration flashes are not considered in the total flash rate, 146.2 moles of NO are produced per flash on average. If the total amount of NO produced by lightning is divided by the total flash rate (4253), one flash produces on average 120.6 moles of NO which is fairly similar to the average NO production rate in the REF simulation (121.3 moles of NO per flash).

If short duration flashes are assumed to produce as many molecules per meter of flash as a normal flash, their impact on the NO mixing ratio is not significant. In Figs. 5 and 8, the NO_SDF and REF simulations give similar results. As noted in the previous section, the simulated short flashes are mostly produced at altitudes between 11 and 12 km m.s.l., which is higher than in the observations.

Because the NO_SDF simulation gives similar results to the REF simulation and the contribution of short flashes to the NO production is small in the REF simulation (2% of LNO_x is from flashes <1 km), the impact of short flashes is not significant. However, it must be kept in mind that little is known about the physics of these discharges. Thus, the impact of the short duration flashes on the NO budget should be studied further when more measurements of short duration flashes are available in conjunction with chemistry data.

5.6 Spatial distribution of the NO molecules

Previous parameterizations (Pickering et al., 1998; DeCaria et al., 2000, 2005) assumed that the NO molecules produced by the lightning flashes are instantly diluted over the whole volume of the cloud or in the 20 dBZ contour. This instant dilution does not produce the NO peaks observed by instruments onboard airplanes (Barth et al., 2007b; Ott et al., 2007). The goal of these sensitivity tests is to investigate how the NO mixing ratio is affected by an instantaneous dilution of the LNO_x source.

Four sensitivity tests are compared to the REF simulation. As in the REF simulation, only *IC* flashes are considered. First, the approach of DeCaria et al. (2005) is followed (VOL_20_DC, Table 1). The NO molecules are distributed vertically following two modes in the volume where the radar reflectivity exceeds 20 dBZ. Second, the NO molecules are

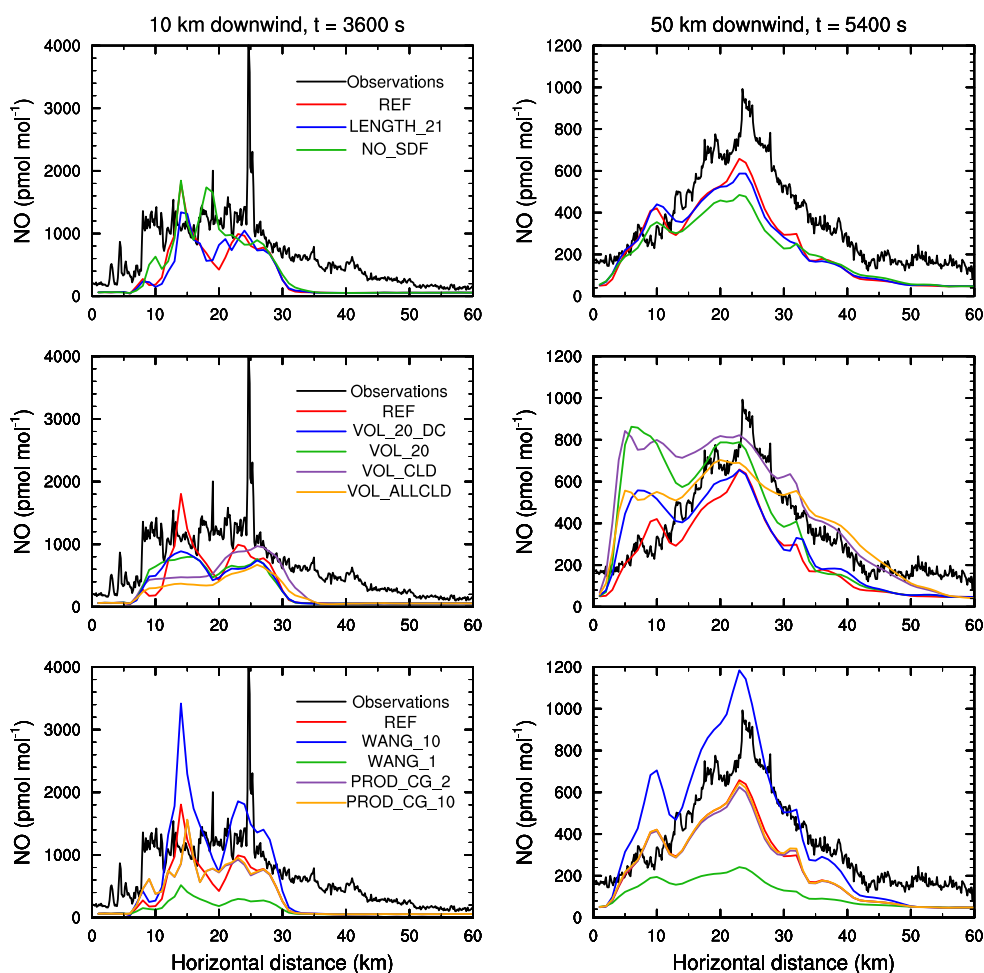


Fig. 7. Same as Fig. 6, for additional simulations.

distributed uniformly in the 20 dBZ volume above the -15°C isotherm (VOL_20). Third, the simulation VOL_CLD follows Pickering et al. (1998) where the LNO_x is distributed over the entire cloud above the -15°C isotherm. In these first three simulations the LNO_x source is only distributed in the detected electrified cell in proportion to the flash rate of each cell. Finally, the last simulation (VOL_ALLCLD) follows Pickering et al. (1998) like VOL_CLD but there is no cell identification. In these four simulations, the flash length is held constant (21 km) since the sensitivity test in Sect. 5.4 has shown no significant impact of the flash length distribution. In the VOL_20_DC, VOL_20, VOL_CLD and VOL_ALLCLD, the NO molecules produced by a single flash are distributed over 9400, 4300, 17 700 and 23 400 grid points on average, respectively. In contrast, the REF simulation places NO by a single flash on ~ 20 grid points.

To identify the impact of the bimodal distribution on the NO mixing ratio, the results of the VOL_20_DC and VOL_20 simulations are compared. In Fig. 5, the cross section of NO

mixing ratio across the anvil for VOL_20_DC is fairly similar to REF. The region of high NO mixing ratio is much larger in VOL_20 than in VOL_20_DC. The study of VOL_CLD and VOL_ALLCLD results gives some insight on the impact of the cell identification. Figure 5 shows that three different spots of NO mixing ratio higher than 540 pmol mol^{-1} are visible for VOL_CLD. In VOL_ALLCLD there is only one large region where the NO mixing ratio exceeds 540 pmol mol^{-1} . When the vertical distribution of the NO molecules is uniform (VOL_20, VOL_CLD, VOL_ALLCLD), the region with high NO mixing ratio across the anvil (Fig. 5) increases with the volume in which NO molecules are instantly diluted. Moreover this volumetric distribution of the NO molecules over a large area does not allow the peaks in the transects to be reproduced near the convective core where an enhancement in the NO mixing ratio is observed (Fig. 7). In these transects (Fig. 7), the NO mixing ratios near the convective core for VOL_20, VOL_20_DC, VOL_CLD and VOL_ALLCLD are lower than observations, but are similar

in magnitude to the observations 50 km downwind of the convective core. The high NO mixing ratios on the southwest side of the transect (Fig. 7, right column) are due to the widespread distribution of the LNO_x source prescribed to be in the cloud or in the 20 dBZ contour.

The NO_x flux in all these simulations is larger than that determined from the observations and in the REF simulation (Table 2) because the NO lightning sources for the VOL_20_DC, VOL_20, VOL_CLD, VOL_ALLCLD simulations are placed at thousands of grid points, many of which are near and within the anvil (see 20 dBZ contour in Fig. 1). The VOL_20_DC NO_x flux is similar to that predicted by other models simulating this storm (Barth et al., 2007b) indicating that their overprediction of the NO_x flux may be due to the larger region of the NO lightning source compared to the filamentary region in the REF simulation. Despite the significant differences in the NO_x flux, the total amount of NO produced from lightning is fairly similar among these 4 sensitivity simulations and the REF simulation.

5.7 Production of NO per flash

A recent review of lightning production of NO reported that the LNO_x production rate per flash length varies from 1×10^{21} to 13×10^{21} molecules m⁻¹ (Schumann and Huntrieser, 2007). This large range of values has been obtained in different storms by different ways: laboratory experiments, modeling studies with different models and different parameterizations or airborne measurements. Barth et al. (2007b) have also reported a large range of NO moles produced per flash (between 36 and 465 moles of NO per IC flash) for the same storm simulated here but using different models and different parameterizations.

The impact of the number of NO molecules produced per flash length unit is investigated in this section. All the simulations use the Wang et al. (1998) equation giving the number of molecules produced per meter of flash (Eq. 2). The WANG_1 simulation uses the original *a* and *b* parameters (see Sect. 2), whereas the REF and WANG_10 simulations use 5 and 10 times the parameters, respectively.

This sensitivity analysis is the one that impacts most the NO mixing ratio both near the convective core and in the anvil. Figure 5 shows that the NO mixing ratio in the anvil in the WANG_10 simulation is far too high compared to observations. In WANG_10, there is a large region with NO mixing ratio higher than 540 pmol mol⁻¹ that extends over 50 km horizontally. Conversely, the WANG_1 simulation exhibits NO mixing ratio in the anvil less than 300 pmol mol⁻¹.

The large difference in the NO mixing ratio between the WANG_1, REF and WANG_10 simulations can be also seen in Fig. 7. The NO moles per flash, the NO peak value, and the total amount of LNO_x produced during the storm increase quasi-linearly as the *a* and *b* parameters increase (Table 2). The NO mixing ratio increase is not exactly linear since it is impacted by the NO_x chemistry. The values of the LNO_x

average profiles are affected by changing the *a* and *b* parameters, but the trends are the same for the three simulations (Fig. 8).

Two additional simulations are performed to study the impact of a larger NO production rate by CG flashes. Pickering et al. (1998) used the values given by Price et al. (1997) (111 mol(NO) IC⁻¹ and 1113 mol(NO) CG⁻¹) to simulate seven case studies representing different environments. Following the method of Price et al. (1997) to determine the amount of NO produced per flash in the 21 July EULINOX storm, Fehr et al. (2004) used the value of 350 mol(NO) CG⁻¹. The 480 moles of NO produced per IC were obtained by a fit to observations. DeCaria et al. (2005) who simulated the 12 July 1996 STERAO storm using the GCE model with the Price et al. (1997) method determined that the IC mean production rate is 460 moles of NO per IC flash. They also concluded from their sensitivity tests that IC and CG flashes produce the same amount of NO per flash. However, they assumed an instantaneous dilution of the NO molecules and only compared with the column NO_x mass from observations. Ott et al. (2007) deduced from their study that 360 moles of NO for both IC and CG flash matches best with observations. Thus, the value of 121 moles of NO produced per flash derived here for the 10 July 1996 STERAO storm is in the lower range of values used or deduced from previous CRM studies except when an explicit electrical scheme is used. In previous parameterizations, the number of NO moles per flash was mostly deduced from Price et al. (1997) who suggested a ratio of 10 between the production rate per CG and IC, or it was deduced from observations, but only in one part of the storm. Few of the previous studies have used a geometric approach for the flash segments distribution or compared the NO mixing ratio to observations in different regions of the storm.

The impact of the NO production rate per IC and CG is investigated with simulations PROD_CG_2 and PROD_CG_10. In these sensitivity tests, the number of NO molecules produced per meter of flash in a CG flash for a particular altitude is multiplied by 2 (PROD_CG_2) and 10 (PROD_CG_10) compared to an IC flash. In PROD_CG_2, the *a* and *b* coefficients of Eq. 2 are 3.4×10^{21} and 13.0×10^{16} respectively for CG flashes. For the PROD_CG_10, these coefficients become 1.7×10^{22} and 6.5×10^{17} , respectively, for CG flashes. For IC flashes, the *a*_{REF} and *b*_{REF} parameters are used in the two sensitivity tests. The CG flash rate is given by the NLDN observations.

Figures 5, 7 and 8 show no significant influence of increasing the NO production rate per CG flash length by a factor of 2 or 10. The NO_x flux through the anvil in PROD_CG_2 and PROD_CG_10 is higher than in REF where CG flashes are not considered (Table 2). Comparing CG_OBS, PROD_CG_2 and PROD_CG_10 shows an increase in the average number of NO moles per flash and in the NO_x flux through the anvil. The average number of NO moles per flash is increased by 0.5% and 5.4% between CG_OBS and PROD_CG_2, and be-

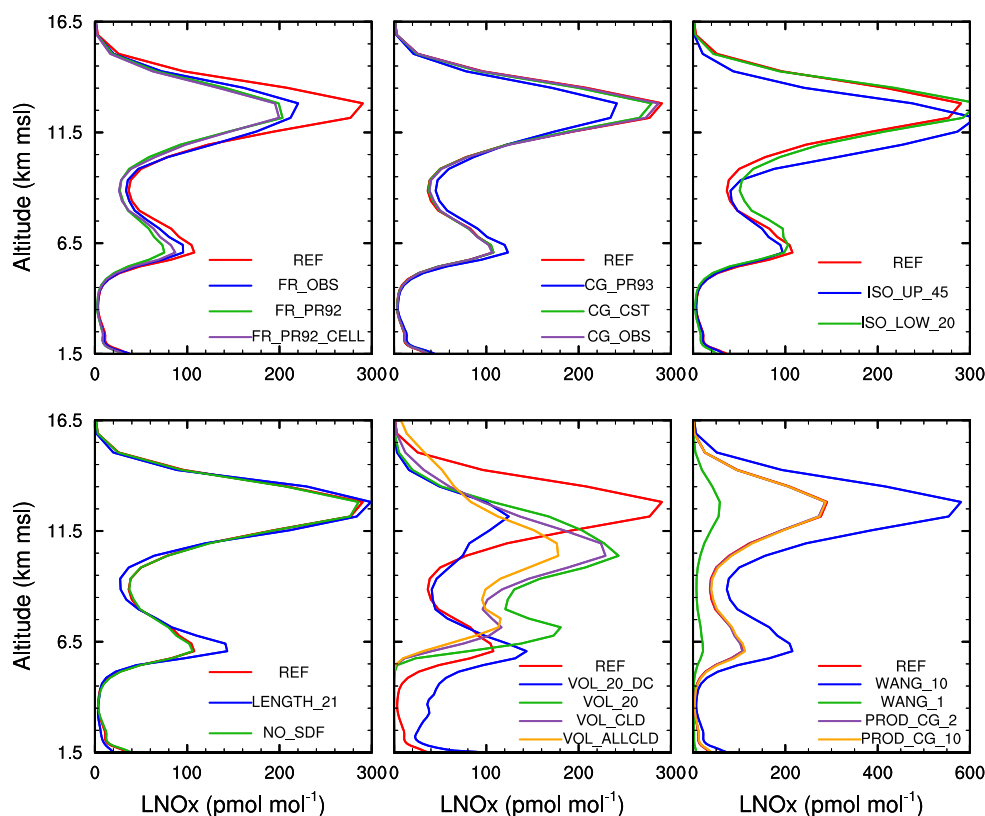


Fig. 8. Domain averaged vertical profiles of the LNO_x tracer at $t=180$ min. The LNO_x tracer corresponds to the NO molecules produced by lightning flashes and transported. The LNO_x tracer does not experience any chemical reaction. The different simulations are defined in Table 1.

tween CG_OBS and PROD_CG_10, respectively. However, because only a small fraction of flashes are CG in this storm, it is difficult to conclude whether the IC and CG NO production ratio is important or not.

6 Conclusions

A new lightning-produced NO_x parameterization has been developed for use in cloud-resolving models. This parameterization is based on three factors: flash rate, spatial distribution and number of NO molecules produced per flash. The flash type is assumed to be intracloud based on observations of the storm simulated in this study. The new lightning-produced NO_x parameterization has three unique characteristics. First, a vertical velocity threshold is used to identify the cells that can produce lightning. Second, the flash rate is estimated from the non-precipitation and precipitation ice mass flux product, which has the benefit of containing information on both the dynamical and microphysical state of the storm. Third, the source location of the NO is filamentary using the approach of Ott et al. (2007). This parameterization has been tested on the 10 July 1996 STERAO storm. The predicted

flash rate is in good agreement with observations for both the magnitude and trend of the flash rate. The distribution of the NO mixing ratio in the anvil, and the NO mixing ratio values near the convective core and in the anvil agree well with the aircraft measurements taken in the 10 July 1996 STERAO storm.

Several sensitivity tests have been performed to determine the parameters that the lightning-produced NO_x parameterization is most dependent upon. The flash rate is an important factor. For these simulations, using the predicted flash rate based on the maximum vertical velocity (Price and Rind, 1992) produced significantly different results from the observations for both flash rate and NO mixing ratios. Using observed flash rate data when available is desirable, but the modeled storm dynamics and physics must reproduce the observations well. For the 10 July 1996 STERAO storm, the duration of each stage of the storm (multicell, transition, supercell) was correlated with the lightning flash rate. Thus, for this case, it is also important to simulate the duration of each stage accurately to have corresponding microphysics and dynamics with observed flash rate.

The spatial placement of the lightning-NO_x source is also an important factor. Placement of NO in large regions of the storm such as within the 20 dBZ contour (DeCaria et al., 2000) or the cloud boundary at temperatures < -15°C (Pickering et al., 1998) resulted in high NO mixing ratios in the anvil region of the storm. Further these previous studies give much higher magnitudes of NO produced per flash than estimated in the current study using a virtual flash path (i.e. small NO source region). The sensitivity of NO to the vertical distribution of the source of NO from lightning was substantial for NO mixing ratios in the anvil. The resulting vertical profiles of NO_x from lightning always had two altitudes of peak NO even when the NO source was uniformly distributed vertically. Thus, lightning-NO_x parameterizations in large scale models (where the convection is parameterized) should represent this NO source in a similar bimodal fashion.

The magnitude of the NO produced per length of flash strongly influences the NO mixing ratio near the convective cores and in the anvil region. Tests with twice the NO produced and with one-fifth the NO produced show a quasi-linear response of NO mixing ratio. Similarly, the produced NO mixing ratio increases linearly with the flash length. Analysis of the model results showed that the longer flashes >30 km contribute most to lightning-produced NO (80%) while flashes <1 km only produce 2% of the lightning-produced NO.

The lightning-produced NO_x parameterization was shown to not be very sensitive to a number of parameters including the cloud-to-ground to intra-cloud lightning ratio, the altitudes (within ~1 km) of the peaks of the NO source, the lightning flash length distribution, the presence of short duration flashes, and the ratio of NO produced by CG lightning to NO produced by IC lightning. Some of these parameters that are sensitive to flash type will likely have a greater influence on NO produced from lightning in other storms because the 10 July 1996 STERAO storm primarily contained intracloud flashes.

These sensitivity simulations can provide guidance for both future modeling and measurement strategies. The storm simulated for this study represented a severe storm occurring in a regime of high cloud bases, high wind shear and convective available potential energy. Storms from other regimes e.g. the southern Great Plains with warmer cloud bases, the airmass thunderstorms typically produced by sea breezes, and tropical storms will be simulated. Despite a number of recent field experiments (STEPS, TROCCINOX, SCOUT-O3, and AMMA), there is still a need for concomitant observations of cloud dynamics, microphysics, electrical activity, and chemistry. In particular, measurements of NO_x near the convective core should be done to pinpoint the spatial extent of the lightning source of NO. The modeling and experimental studies of a variety of storms should then be able to elucidate the amount of NO typically produced from a thunderstorm.

Acknowledgements. We appreciate the comments by B. Ridley, L. Emmons, E. Defer, and two anonymous reviewers on this work. This research has been financially supported by NCAR's Advanced Study Program. The National Center for Atmospheric Research is operated by the University Corporation for Atmospheric Research under the sponsorship of the National Science Foundation.

Edited by: R. Cohen

References

- Barth, M. C., Stuart, A. L., and Skamarock, W. C.: Numerical simulations of the July 10, 1996, Stratospheric-Tropospheric Experiment: Radiation, Aerosols, and Ozone STERAO- Deep convection experiment storm: Redistribution of soluble tracers, *J. Geophys. Res.*, 106(D12), 12 381–12 400, doi:10.1029/2001JD900139, 2001.
- Barth, M. C., Kim, S.-W., Skamarock, W. C., Stuart, A. L., Pickering, K. E., and Ott, L. E.: Simulations of the redistribution of formaldehyde, formic acid, and peroxides in the July 10, 1996 STERAO deep convection storm, *J. Geophys. Res.*, 112, D13310, doi:10.1029/2006JD008046, 2007a.
- Barth, M. C., Kim, S.-W., Wang, C., Pickering, K. E., Ott, L. E., Stenichkov, G., Leriche, M., Cautenet, S., Pinty, J.-P., Barthe, C., Mari, C., Helsen, J., Farley, R., Fridlind, A. M., Ackerman, A. S., Spiridinov, V., and Telenta, B.: Cloud-scale model inter-comparison of chemical constituent transport in deep convection, *Atmos. Chem. Phys.*, 7, 4709–4731, 2007b, <http://www.atmos-chem-phys.net/7/4709/2007/>.
- Barthe, C. and Pinty, J.-P.: Simulation of Electrified Storms with Comparison of the Charge Structure and Lightning Efficiency, *J. Geophys. Res.*, 112, D19204, doi:10.1029/2006JD008241, 2007a.
- Barthe, C. and Pinty, J.-P.: Simulation of a supercellular storm using a three-dimensional mesoscale model with an explicit lightning flash scheme, *J. Geophys. Res.*, 112, D06210, doi:10.1029/2006JD007484, 2007b.
- Barthe, C., Molinié, G., and Pinty, J.-P.: Description and first results of an explicit electrical scheme in a 3D cloud resolving model, *Atmos. Res.*, 76, 95–113, 2005.
- Barthe, C., Deierling, W., and Barth, M. C.: On the use of ice mass fluxes to estimate total lightning in cloud resolving models, *Eos Trans. AGU*, 88(52), Fall Meeting Suppl., Abstract AE43A-02, 2007a.
- Barthe, C., Pinty, J.-P., and Mari, C.: Lightning-produced NO_x in an explicit electrical scheme: a STERAO case study, *J. Geophys. Res.*, 112, D04302, doi:10.1029/2006JD007402, 2007b.
- Blyth Jr., A. M., H. J. C., Driscoll, K., Gadian, A. M., and Latham, J.: Determination of ice precipitation rates and thunderstorm anvil ice contents from satellite observations of lightning, *Atmos. Res.*, 59–60, 217–229, 2001.
- Boccippio, D. J., Cummins, K. L., Christian, H. J., and Goodman, S. J.: Combined satellite- and surface-based estimation of the intracloud-cloud-to-ground lightning ratio over the Continental United States, *Mon. Weather Rev.*, 129, 108–122, 2001.
- Boccippio, D. J., Koshak, W. J., and Blakeslee, R. J.: Performance Assessment of the Optical Transient Detector and Lightning Imaging Sensor. Part I: Predicted Diurnal Variability, *J. Atmos. Oceanic Technol.*, 19, 1318–1332, 2002.

- Bruning, E. C., Rust, W. D., Schuur, T. J., MacGorman, D. R., Krehbiel, P. R., and Rison, W.: Electrical and polarimetric radar observations of a multicell storm in TELEX, *Mon. Weather Rev.*, 135, 2525–2544, 2007.
- Christian, H. J., Blakeslee, R. J., Goodman, S. J., Mach, D. A., Stewart, M. F., Buechler, D. E., Koshak, W. J., Hall, J. M., Boeck, W. L., Driscoll, K. T., and Boccippio, D. J.: The Lightning Imaging Sensor (LIS), paper presented at 11th International Conference on Atmospheric Electricity, Guntersville, Alabama, 1999.
- Cummins, K. L., Murphy, M. J., Bardo, E. A., Hiscox, W. L., Pyle, R. B., and Pifer, A. E.: A combined TOA/MDF technology upgrade of the U.S. National Detection Network, *J. Geophys. Res.*, 103, 9035–9044, 1998.
- DeCaria, A. J., Pickering, K. E., Stenchikov, G. L., Scala, J. R., Stith, J. L., Dye, J. E., Ridley, B. A., and Laroche, P.: A cloud-scale model study of lightning-generated NO_x in an individual thunderstorm during STERAO-A, *J. Geophys. Res.*, 105, 11 601–11 616, 2000.
- DeCaria, A. J., Pickering, K. E., Stenchikov, G. L., and Ott, L. E.: Lightning-generated NO_x and its impact on tropospheric ozone production: A three-dimensional modeling study of a Stratosphere-Troposphere Experiment: Radiation, Aerosols and Ozone (STERAO-A) thunderstorm, *J. Geophys. Res.*, 110, D14303, doi:10.1029/2004JD005556, 2005.
- Defer, E., Blanchet, P., Théry, C., Laroche, P., Dye, J. E., Venticinque, M., and Cummins, K. L.: Lightning activity for the July 10, 1996, storm during the Stratosphere-Troposphere Experiment: Radiation, Aerosol, and Ozone-A (STERAO-A) experiment, *J. Geophys. Res.*, 106, 10 151–10 172, doi:10.1029/2000JD900849, 2001.
- Defer, E., Laroche, P., Dye, J. E., and Skamarock, W. C.: Use of total lightning lengths to estimate NO_x production in a Colorado thunderstorm, in: Proceedings of the 12th International Conference on Atmospheric Electricity, 9–13 June 2003, Int. Comm. on Atmos. Electr., Versailles, France, 2003.
- Defer, E., Blanchet, P., and Laroche, P.: Ground based VHF and space borne optical measurements of lightning flashes during the STERAO-A experiment, in: The Lightning Imaging Sensor International Workshop, 11–14 September 2006, Huntsville, Alabama, 2006.
- Deierling, W.: The relationship between total lightning and ice fluxes, Ph.D. thesis, University of Alabama, Huntsville, Alabama, 2006.
- Dye, J. E., Ridley, B. A., Skamarock, W., Barth, M., Venticinque, M., Defer, E., Blanchet, P., Théry, C., Laroche, P., Baumann, K., Hubler, G., Parrish, D. D., Ryerson, T., Trainer, M., Frost, G., Holloway, J. S., Matejka, T., Bartels, D., Fehsenfeld, F. C., Tuck, A., Rutledge, S. A., Lang, T., Stith, J., and Zerr, R.: An overview of the Stratospheric-Tropospheric Experiment: Radiation, Aerosols, and Ozone (STERAO)-Deep Convection experiment with results for the July 10, 1996 storm, *J. Geophys. Res.*, 105, 10 023–10 045, doi:10.1029/1999JD901116, 2000.
- Fehr, T., Höller, H., and Huntrieser, H.: Model study on production and transport of lightning-produced NO_x in a EULINOX supercell storm, *J. Geophys. Res.*, 109, 1–17, doi:10.1029/2003JD003 935, 2004.
- Franzblau, E. and Popp, C. J.: Nitrogen oxides produced from lightning, *J. Geophys. Res.*, 94, 11 089–11 104, 1989.
- Harlin, J. D., Hamlin, T., Krehbiel, P., Thomas, R., and Rison, W.: Short duration discharges located by NMIMT's Lightning Mapping Array, in: Fall meeting, December 2003, American Geophysical Union, San Francisco, CA, 2003.
- Helsdon, J. H., Wu, G., and Farley, R. D.: An intracloud lightning parameterization scheme for a storm electrification model, *J. Geophys. Res.*, 97, 5865–5884, 1992.
- Höller, H., Finke, U., Huntrieser, H., Hagen, M., and Feigl, C.: Lightning-produced NO_x (LINOX): experimental design and case study results, *J. Geophys. Res.*, 104, 13 911–13 922, doi:10.1029/1999JD900019, 1999.
- Huntrieser, H., Feigl, C., Schlager, H., Schroder, F., Gerbig, C., van Velthoven, P., Flatoy, F., Théry, C., Petzold, A., Höller, H., and Schumann, U.: Airborne measurements of NO_x, tracer species and small particles during the European Lightning Nitrogen Oxides Experiment, *J. Geophys. Res.*, 107(D11), 4113, doi:10.1029/2000JD000209, 2002.
- Jayarathne, R., Saunders, C. P. R., and Hallet, J.: Laboratory studies of the charging of soft hail during ice crystal interactions, *Q. J. Roy. Meteor. Soc.*, 103, 609–630, 1983.
- Krehbiel, P., Thomas, R. J., Rison, W., Hamlin, T., Harlin, J., and Davis, M.: Lightning mapping observations in Central Oklahoma, *Eos*, pp. 21–25, 2000.
- Kuhlman, K. M., Ziegler, C. L., Mansell, E. R., MacGorman, D. R., and Straka, J. M.: Numerically simulated electrification and lightning of the 29 June 2000 STEPS supercell storm, *Mon. Weather Rev.*, 134(10), 2734–2757, 2005.
- Lang, T. J., Rutledge, S. A., Dye, J. E., Venticinque, M., Laroche, P., and Defer, E.: Anomalously low negative cloud-to-ground lightning flash rates in intense convective storms observed during STERAO-A, *Mon. Weather Rev.*, 128, 160–173, 2000.
- Latham, J., Petersen, W. A., Deierling, W., and Christian, H. J.: Field identification of a unique globally dominant mechanism of thunderstorm electrification, *Q. J. Roy. Meteor. Soc.*, 133, 1453–1457, 2007.
- Lin, Y.-L., Farley, R. D., and Orville, H. D.: Bulk parameterization of the snow field in a cloud model, *J. Clim. Appl. Meteor.*, 22, 1065–1092, 1983.
- MacGorman, D. R., Burgess, D. W., Mazur, V., Rust, W. D., Taylor, W. L., and Johnson, B. C.: Lightning rates relative to tornadic storm evolution on 22 May 1981, *J. Atmos. Sci.*, 46, 221–250, 1989.
- Mansell, E. R., MacGorman, D., Ziegler, C. L., and Straka, J. M.: Simulated three-dimensional branched lightning in a numerical thunderstorm model, *J. Geophys. Res.*, 107(D9), 4075, doi:10.1029/2000JD000244, 2002.
- Ott, L. E., Pickering, K. E., Stenchikov, G., Huntrieser, H., and Schumann, U.: Effects of lightning NO_x production during the 21 July European Lightning Nitrogen Oxides Project storm studied with a three-dimensional cloud-scale chemical transport model, *J. Geophys. Res.*, 112, D05307, doi:1029/2006JD007365, 2007.
- Pickering, K. E., Wang, Y., Tao, W. K., Price, C., and Müller, J.-F.: Vertical distributions of lightning NO_x for use in regional and global chemical transport models, *J. Geophys. Res.*, 103, 31 203–31 216, 1998.
- Pinty, J.-P. and Barthe, C.: Ensemble simulation of the lightning flash variability in a 3-D cloud model with parameterizations of cloud electrification and lightning flashes, *Mon. Weather Rev.*, 136, 380–387, 2008.

- Popp, P. J., Gao, R. S., Marcy, T. P., Fahey, D. W., Hudson, P. K., Thompson, T. L., Krcher, B., Ridley, B. A., Weinheimer, A. J., Knapp, D. J., Montzka, D. D., Baumgardner, D., Garrett, T. J., Weinstock, E. M., Smith, J. B., Sayres, D. S., Pittman, J. V., Dhaniala, S., Bui, T. P., and Mahoney, M. J.: Nitric acid uptake on subtropical cirrus cloud particles, *J. Geophys. Res.*, 109, D06302, doi:10.1029/2003JD004255, 2004.
- Price, C. and Rind, D.: A simple lightning parameterization for calculating global lightning distributions, *J. Geophys. Res.*, 97, 9919–9933, 1992.
- Price, C. and Rind, D.: What determines the cloud-to-ground lightning fraction in thunderstorms?, *Geophys. Res. Lett.*, 20, 463–466, 1993.
- Price, C., Penner, J., and Prather, M.: NO_x from lightning. 1. Global distribution based on lightning physics, *J. Geophys. Res.*, 102, 5929–5941, 1997.
- Proctor, D. E.: VHF radio pictures of cloud flashes, *J. Geophys. Res.*, 86, 4041–4071, 1981.
- Ridley, B. A., Pickering, K. E., and Dye, J. E.: Comments on the parameterization of lightning-produced NO in global chemistry-transport models, *Atmos. Environ.*, 39, 6184–6187, 2005.
- Rison, W., Thomas, R. J., Krehbiel, P. R., Hamlin, T., and Harlin, J.: A GPS-based three-dimensional lightning mapping system : initial observations in Central New-Mexico, *Geophys. Res. Lett.*, 26, 3573–3576, 1999.
- Salzmann, M., Lawrence, M. G., Phillips, V. T. J., and Donner, L. J.: Cloud system resolving model study of the roles of deep convection for photo-chemistry in the TOGA COARE/CEPEX region, *Atmos. Chem. Phys.*, 8, 2741–2757, 2008, <http://www.atmos-chem-phys.net/8/2741/2008/>.
- Saunders, C. P. R., Keith, W. D., and Mitzeva, R. P.: The effect of liquid water on thunderstorm charging, *J. Geophys. Res.*, 96, 11 007–11 017, 1991.
- Schumann, U. and Huntrieser, H.: The global lightning-induced nitrogen oxides source, *Atmos. Chem. Phys.*, 7, 3823–3907, 2007, <http://www.atmos-chem-phys.net/7/3823/2007/>.
- Shao, X. M. and Krehbiel, P. R.: The spatial and temporal development of intracloud lightning, *J. Geophys. Res.*, 101, 26 641–26 668, 1996.
- Skamarock, W. C., Powers, J. G., Barth, M., Dye, J. E., Matejka, T., Bartels, D., Baumann, K., Stith, J., Parrish, D. D., and Hübler, G.: Numerical simulations of the July 10 Stratospheric-Tropospheric Experiment: Radiation, Aerosol, and Ozone/Deep Convection Experiment convective system: Kinematics and transport, *J. Geophys. Res.*, 105, 19973–19990, 2000.
- Skamarock, W. C., Dye, J. E., Defer, E., Barth, M. C., Stith, J. L., and Ridley, B. A.: Observational- and modeling-based budget of lightning-produced NO_x in a continental thunderstorm, *J. Geophys. Res.*, 108(D10), 4305, doi:10.1029/2002JD002163, 2003.
- Skamarock, W. C., Klemp, J. B., Dudhia, J., Gill, D., Barker, D., Wang, W., and Powers, J. G.: A description of the Advanced Research WRF Version 2, Tech. Rep. NCAR/TN468+STR, NCAR, Boulder, Colorado, 2005.
- Stith, J., Dye, J., Ridley, B., Laroche, P., Defer, E., Baumann, K., Hübler, G., Zerr, R., and Venticinque, M.: NO signatures from lightning flashes, *J. Geophys. Res.*, 104, 16 081–16 089, 1999.
- Stolzenburg, M., Rust, W. D., and Marshall, T. C.: Electrical structure in thunderstorm convective regions – 3. Synthesis, *J. Geophys. Res.*, 103, 14 097–14 108, 1998.
- Tabazadeh, A., Toon, O. B., and Jensen, E. J.: A surface chemistry model for nonreactive trace gas adsorption on ice: Implications for nitric acid scavenging by cirrus, *Geophys. Res. Lett.*, 26(14), 2211–2214, doi:10.1029/1999GL900501, 1999.
- Takahashi, T.: Riming electrification as a charge generation mechanism in thunderstorms, *J. Atmos. Sci.*, 35, 1536–1548, 1978.
- Théry, C., Laroche, P., and Blanchet, P.: EULINOX – The European Lightning Nitrogen Oxides Experiment, Rep. DLR-FB 2000-28, edited by: Höller, H. and Schumann, U., Deutsches Zentrum für Luft- und Raumfahrt, Köln, Germany, 2000.
- Thomas, R. J., Krehbiel, P. R., Rison, W., Hamlin, T., Harlin, J., and Shown, D.: Observations of VHF source powers radiated by lightning, *Geophys. Res. Lett.*, 28, 143–146, 2001.
- Ushio, T., Heckman, S. T., Christian, H. J., and Kawasaki, Z.-I.: Vertical development of lightning activity observed by the LDAR system: lightning bubbles, *J. Appl. Meteor.*, 42, 165–174, 2003.
- Wang, C. and Chang, J.: Three-dimensional numerical model of cloud dynamics, microphysics, and chemistry 1. Concepts and formulation, *J. Geophys. Res.*, 98, 14 827–14 844, 1993.
- Wang, C. and Prinn, R.: On the roles of deep convection clouds in tropospheric chemistry, *J. Geophys. Res.*, 105, 3399–3418, 2000.
- Wang, Y. A., DeSilva, W., Goldenbaum, G. C., and Dickerson, R. R.: Nitric oxide production by simulated lightning : Dependence on current, energy and pressure, *J. Geophys. Res.*, 103, 19 149–19 159, 1998.
- Wicker, L. J. and Skamarock, W. C.: Time-splitting methods for elastic models using forward time schemes, *Mon. Weather Rev.*, 130, 2088–2097, 2002.
- Wiens, K. C., Rutledge, S. A., and Tessendorf, S. A.: The 29 June 2000 supercell observed during STEPS. Part II: Lightning and charge structure, *J. Atmos. Sci.*, 62, 4151–4177, 2005.
- Zhang, X., Helsdon, J. H., and Farley, R. D.: Numerical modeling of lightning-produced NO_x using an explicit lightning scheme: 2. Three-dimensional simulation and expanded chemistry, *J. Geophys. Res.*, 108(D18), A21–A37, doi:10.1029/2002JD003225, 2003.
- Zipser, E. J. and Lutz, K. R.: The vertical profile of radar reflectivity of convective cells: a strong indicator of storm intensity and lightning probability?, *Mon. Weather Rev.*, 122, 1751–1759, 1994.